

Actin Cross-Linkers and the Shape of Stereocilia

Martin Lenz,^{†‡§*} Jacques Prost,^{†‡¶} and Jean-François Joanny^{†‡§}

[†]Institut Curie, Centre de Recherche, Laboratoire Physico-Chimie Curie, Paris, France; [‡]Centre National de la Recherche Scientifique, UMR 168, Paris, France; [§]Université Pierre et Marie Curie-Paris 6, UMR 168, Paris, France; and [¶]École Supérieure de Physique et de Chimie Industrielles—ParisTech, Paris, France

ABSTRACT Stereocilia are actin-based cellular protrusions essential for hearing. We propose that they are shaped by the detachment dynamics of actin cross-linkers, in particular espin. We account for experimentally observed stereocilium shapes, treadmill velocity to length relationship, espin 1 localization profile, and microvillus length to espin level relationship. If the cross-linkers are allowed to reattach, our model yields a dynamical phase transition toward unbounded growth. Considering the simplified case of a noninteracting, one-filament system, we calculate the length probability distribution in the growing phase and its stationary form in a continuum approximation of the finite-length phase. Numerical simulations of interacting filaments suggest an anomalous power-law divergence of the protrusion length at the growth transition, which could be a universal feature of cross-linked depolymerizing systems.

INTRODUCTION

The exquisite frequency selectivity of our hearing can be tracked back to the intricate and remarkably well-regulated internal structure of the ear. At the heart of this mechano-transduction machinery are stereocilia, which are present in reptiles, birds, and mammals. They are 1–120 μm -long rodlike protrusions of so-called hair cells that pivot around their ankle upon mechanical stimulation (1). This motion causes the opening of ion channels, which induces a depolarization of the membrane that results in the propagation of a nervous signal. Stereocilia are primarily made of a paracrystal of up to 200 densely packed (2), parallel actin filaments enclosed by the cell membrane (3). They are roughly cylindrical over most of their length, but taper at their base. This indicates that some filaments do not extend all the way to the cell body, although some others do penetrate far into the underlying cuticular plate (see Fig. 1 *b*). Within the stereocilium the filaments are in register, meaning that their helical periods are perfectly aligned in the vertical direction. Their barbed (polymerizing) ends point toward the stereocilium tip while their depolymerizing ends point toward the cell body. Although stereocilia are maintained throughout the life span of an individual, they are dynamic structures that are constantly renewed by actin treadmill. During this process, actin is continuously incorporated at the tip of the stereocilium and depolymerized at its base (4). Interestingly, the actin treadmill velocity is proportional to the stereocilium height, so that the time necessary to fully renew any auditory stereocilium is independent of the stereocilium height (it has been shown to be ≈ 48 h in rats (5)).

Stereocilia have recently been the focus of theoretical attention (6,7), and two of us have suggested that this

renewal time is essentially an intrinsic timescale associated with the actin bundle's depolymerization dynamics (8). However, the origin of the timescale proposed in this previous work yields a strong sensitivity of the stereocilium shape on the model's parameters. In addition, this model does not account well for the long quasicylindrical section observed in healthy stereocilia. Here we improve the notion of an intrinsic timescale put forward in Prost et al. (8) by suggesting that it originates in the binding-unbinding dynamics of actin cross-linkers, which were mentioned but not treated explicitly in this work. Our description of this experimentally well-characterized mechanism allows us to reproduce stereocilium shapes faithfully with few adjustable parameters and to quantitatively account for experimental results previously only considered from a qualitative point of view. Finally, it yields robust structures, which is very significant because the frequency sensitivity of the ear requires a delicate regulation of the stereocilia's mechanical properties, which are in turn determined by their shape.

Actin cross-linking was described early in the study of stereocilia (9) and could be responsible for the filaments being in register (10). Although cross-linkers of two types, espin and fimbrin, have been identified in stereocilia (11,12), we hereafter focus on espin, which is thought to provide sturdier cross-linking than fimbrin (13,14). Note, however, that our study is general enough to apply to any cross-linker, and could be extended to account for the simultaneous presence of several cross-linker species. Espin slows actin depolymerization down in vitro (15), and could thus play an important role in stereocilia, as the actin depolymerization rate there ($\approx 0.002\text{--}0.04$ s^{-1} over the whole stereocilium, meaning $\approx 10^{-4}$ s^{-1} for each filament (5)) is much smaller than that of F-actin in vitro (≈ 1 s^{-1} (16)). Several in vivo experiments indeed support the notion that cross-linking plays a major role in the length regulation of

Submitted April 8, 2010, and accepted for publication July 28, 2010.

*Correspondence: martinlenz@uchicago.edu

Editor: Denis Wirtz.

© 2010 by the Biophysical Society
0006-3495/10/10/2423/11 \$2.00

doi: 10.1016/j.bpj.2010.07.065

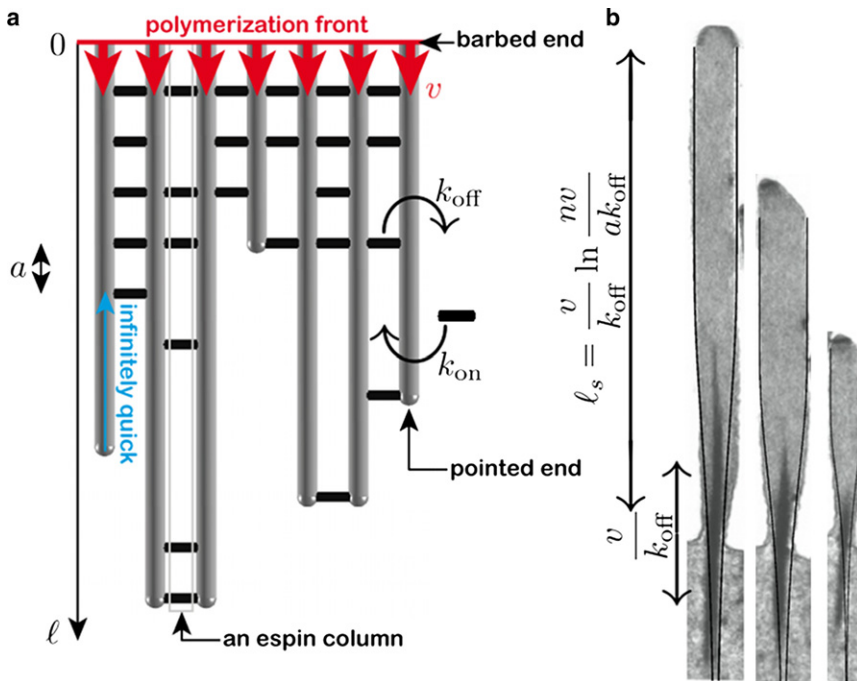


FIGURE 1 Model stereocilium and comparison with experimental shapes. (a) Cross-linked actin is produced in $l = 0$ and treadmills down with a velocity v . Meanwhile, espins are exchanged with the surrounding solution with rates k_{on} and k_{off} . An actin filament not held by a cross-linker at its pointed end immediately depolymerizes to the next espin. (b) Comparison between our predictions (Eq. 4, plotted as *thick black lines*, the top ends of which indicate $l = 0$, the polymerization front), and three guinea pig stereocilia from the same hair cell (*micrographs* taken from Fig. 3 a of (25)). Note the stereocilia's long cylindrical top section, tapered base, and the fact that they insert into the cuticular plate (the top part of cell body). The diameter of the tallest stereocilium is ~ 250 nm.

stereocilia and related cellular protrusions. When transfected with espin, LLC-PK1-CL4 epithelial cells (referred to as CL4 cells in the following) undergo a dramatic lengthening of one such type of protrusions, microvilli, which could be due to espin preventing their disassembly (17). Other actin cross-linkers are also known to inhibit the disassembly of actin bundles in *Drosophila* bristle (18). Espin is incorporated at the stereocilium tip and treadmills down simultaneously with actin (5). Its overexpression (but not that of actin) induces the lengthening of stereocilia and a mutation resulting in espin underexpression causes their shortening (19). Under normal *in vivo* conditions, the variability in stereociliar length is correlated with the espin expression level (15,20) and isoform expression pattern (21). Finally, two recessive and four dominant mutations of espin are responsible for deafness in humans (13). Out of the four dominant ones, three induce less microvillus lengthening than wild-type espin when transfected into CL4 cells (17).

This article is organized as follows. In Model for the Actin and Cross-Linker Dynamics, we present a model for the coupled dynamics of espin cross-linking and actin depolymerization. Solving the simple case where espin is incorporated into the actin bundle only at the tip of stereocilia, we show in Stereocilium Shape without Espin Reattachment that our formalism yields robust stereocilia shapes with only one adjustable parameter and accounts for experimental results not previously discussed in the theoretical literature. In Single Filament with Reattachment, we show the modifications induced by espin reattachment during the course of treadmilling by discussing a simplified situation involving only one filament. Coupling Between

Filaments then focuses on the lateral correlations that espin reattachment induces in a multifilament bundle, and we discuss our results in the last section, Discussion and Conclusions.

MODEL FOR THE ACTIN AND CROSS-LINKER DYNAMICS

Our model is presented in Fig. 1 a. Completely cross-linked actin is continuously produced at a location $l = 0$ with an externally imposed treadmilling velocity v , the regulation of which is discussed in Prost et al. (8). The polymerization dynamics of the actin bundle is thus assumed to be deterministic. In practice, this polymerization is highly regulated by several proteins comprised in the electron-dense tip complex located at the stereocilium tip (19,22–24). Because the filaments across the bundle are cross-linked, they move together at a velocity equal to the average polymerization rate of the filaments. As there are many filaments in the bundle, the fluctuations of this average should be small.

As actin moves down, espin is exchanged with the surrounding medium. Considering that the typical time for the depolymerization dynamics in stereocilia is ≈ 1000 s (the time required to depolymerize one helical period of the actin filament according to (25)) and assuming a diffusion constant of $60 \mu\text{m}^2 \cdot \text{s}^{-1}$ (estimated from the Stokes radius of espin (26)), we estimate that the unbound espin concentration is homogeneous over length scales of order at least $250 \mu\text{m}$, i.e., larger than the size of the stereocilium. We thus consider that the espin attachment and detachment rates k_{on} and k_{off} are constant throughout the stereocilium (k_{off} also accounts for espin degradation). Note that this

reasoning would not hold if espin were actively localized in some regions of the stereocilia, or if the diffusion of espin were slowed down considerably, for instance by crowding effects. It is, however, not known how much the actin bundle slows the diffusion of espin down, and we assume throughout this article that this effect is not sufficient to induce significant espin density gradients. The opposite hypothesis is considered in Naoz et al. (7), which we further discuss in the last section. A similar argument applies to the supply of actin to the stereocilium tip, which we consider to always be sufficient to maintain the treadmilling velocity v . Finally, espin attachment at the altitude ℓ is only possible between two neighboring filaments of length equal to or larger than ℓ , as espin cannot reattach if there are no actin filaments.

We formulate the simplifying hypothesis that actin filaments can only depolymerize from their pointed ends. In agreement with the experimental results presented in the previous section, we assume that espin prevents the depolymerization of the actin filaments that it cross-links. Furthermore, we assume that the depolymerization of actin alone happens on much shorter timescales (≈ 1 s) than the espin detachment dynamics (≈ 1000 s). Hence, on the time-scales relevant for the morphogenesis of stereocilia, actin filaments depolymerize instantaneously up to the next point where they are cross-linked, and are then stalled until the detachment of the cross-linker, which occurs at a rate k_{off} . We denote by a the vertical spacing between two actin cross-linkers (see Fig. 1 a). A filament cannot depolymerize beyond $\ell = 0$ (this description is justified if, for instance, a filament of vanishing length is immediately renucleated by the tip complex so that the total number of filaments is conserved).

From the model described here, we expect the lower end of the actin bundle to have a very irregular shape due to the stochastic character of the espin detachment and subsequent actin depolymerization (as in Fig. 1 a, for example). However, we show in the Supporting Material that membrane tension pushes the filaments together, so that they are always in close contact (see Fig. S1 in the Supporting Material).

Unless otherwise specified, in the following we express lengths in units of the distance a between espin sites and times in units of the average cross-linker lifetime k_{off}^{-1} . We denote the dimensionless polymerization velocity $v/(ak_{\text{off}})$ by ν , and define $k = k_{\text{on}}/k_{\text{off}}$.

STEREOCILIAM SHAPE WITHOUT ESPIN REATTACHMENT

In this section we solve our model in the case where espin is incorporated in the actin bundle only at the stereocilium tip ($k = 0$). In this situation, an espin attachment site located at a distance ℓ from the polymerization front is occupied if and only if an espin has been incorporated when this

site was located at the polymerization front and has then survived detachment for a time ℓ/ν . Because the detachment process is analogous to a radioactive decay-like stochastic process with rate 1, the site in question is occupied with probability

$$P_{\text{on}}(\ell) = P_0 e^{-\ell/\nu}, \quad (1)$$

where $P_{\text{on}}(0) = P_0$ is the probability with which an espin cross-linker is incorporated at $\ell = 0$. For a maximally cross-linked bundle, $P_0 = 1$. Now considering not one espin site, but a full espin column (defined in Fig. 1 a), we ask for the probability that the lowermost espin of the column is located at a distance ℓ or smaller from the polymerization front. This probability is given by the infinite product

$$P_c^{\leq}(\ell) = [1 - P_{\text{on}}(\ell + 1)] \times [1 - P_{\text{on}}(\ell + 2)] \times [1 - P_{\text{on}}(\ell + 3)] \times \dots, \quad (2)$$

where $\ell \geq 0$. Now turning to the actin filaments, we see that an actin filament has a length smaller or equal to ℓ if and only if all neighboring espin columns have their lowermost espin at a location $\ell' \leq \ell$. Denoting by n the number of neighbors of an actin filament (filaments are hexagonally packed in mammalian and bird stereocilia so that $n = 6$ (10); $n = 2$ in Fig. 1 a), the probability for a filament to have a length smaller than or equal to ℓ in the absence of espin reattachment reads

$$P_f^{\leq}(\ell) = P_c^{\leq}(\ell)^n = \prod_{i=1}^{+\infty} [1 - P_0 e^{-(\ell+i)/\nu}]^n. \quad (3)$$

We now discuss this result and compare it to experimental data. For the sake of clarity, in the remainder of this section we go back to nonscaled units. Qualitatively, $P_f^{\leq}(\ell)$ is equal to 0 for small ℓ -values, and to 1 for large ℓ -values. If a large number of filaments are present, the number of filaments of length larger than ℓ is proportional to

$$P_f^{>}(\ell) = 1 - P_f^{\leq}(\ell).$$

Because the filaments are closely packed as discussed in Model for the Actin and Cross-Linker Dynamics and in Section S1 in the Supporting Material, the section $\pi[r(\ell)]^2$ of the stereocilium at position ℓ is proportional to the number of filaments longer than ℓ , so that

$$r(\ell) = r(0) \sqrt{1 - P_f^{\leq}(\ell)}. \quad (4)$$

Here we do not specify the physical processes imposing $r(0)$, the radius at the polymerizing end of the actin bundle. For relatively short-lived actin-based protrusion, $r(0)$ could be fixed by dynamical processes operating during the initial actin bundling phase (27). In stereocilia, mechanical effects within the tip complex might lead to its continuous regulation (8). Because the length of the stereocilia ($\approx 5 \mu\text{m}$) is

much larger than that the distance between two cross-linking sites (≈ 10 nm), we can use the continuum limit of Eq. 3,

$$P_f^{\leq}(\ell) \underset{v/(ak_{\text{off}}) \gg 1}{\sim} \exp[-e^{-(\ell-\ell_s)k_{\text{off}}/v}], \quad (5)$$

where

$$\ell_s = \frac{v}{k_{\text{off}}} \ln\left(\frac{nvP_0}{ak_{\text{off}}}\right) \quad (6)$$

(see Sec. S3.3 in the [Supporting Material](#) for a rigorous discussion of this limit). For small values of ℓ , this equation yields a cylindrical profile with a characteristic length ℓ_s given by Eq. 6. The cylinder then tapers over a length v/k_{off} . These predictions are plotted and compared to actual stereocilia shapes in Fig. 1 b. Several parameters involved in our theoretical shapes are well-known experimentally. Up to six espins can bind to each helical period of the actin filament, which yields $a/n = (37/6) \mu\text{m}$ (10). The actin of the part of the stereocilium that sticks out of the cell is completely renewed by treadmilling in $48 \text{ h} = \ell_s/v$ (5), which imposes a different value of v depending on the length of the stereocilium. In agreement with electron microscopy studies, we assume that the actin bundle is heavily cross-linked by espin, so that $P_0 = 1$. This leaves only one free parameter k_{off} . Because the three stereocilia of Fig. 1 b belong to the same cell, we furthermore impose that they are all described by the same value of k_{off} . Taking $k_{\text{off}} = 0.14 \text{ h}^{-1}$ yields a good fit for all three stereocilia.

More quantitative experimental results are also accounted for by our model. First, the relationship Eq. 6 between ℓ_s and v is almost linear, and we show in Fig. 2 a that it is compatible with the observation that the stereocilium's treadmilling velocity is roughly proportional to its length (5). Here the value of k_{off} is the same as the one determined in Fig. 1 b, meaning that no adjustable parameter is used in Fig. 2 a. In Fig. 2 b, we compare the experimentally measured (24) density profile of one specific type of espin, espin 1, along three stereocilia belonging to the same vestibular hair cell to an exponential, because the espin density is expected to be proportional to the probability P_{on} defined in Eq. 1 (note that the actin bundle renewal time in vestibular hair cells is 72 h (5)). The decay length of the experimental curves increases with stereocilium length (and therefore treadmilling velocity) as predicted by this equation. Consequently, three different stereocilia of the same cell are again well described by using one common value of k_{off} . Note, however, that although espin 1 does bind actin, its main role could be the regulation of actin polymerization, while other espins might be responsible for most of the cross-linking (B. Kachar, National Institute of Health, private communication, 2009). Another interesting result is presented in Loomis et al. (15). In this study, CL4 cells are transfected with espin, which causes the elongation of the cells' microvilli. The

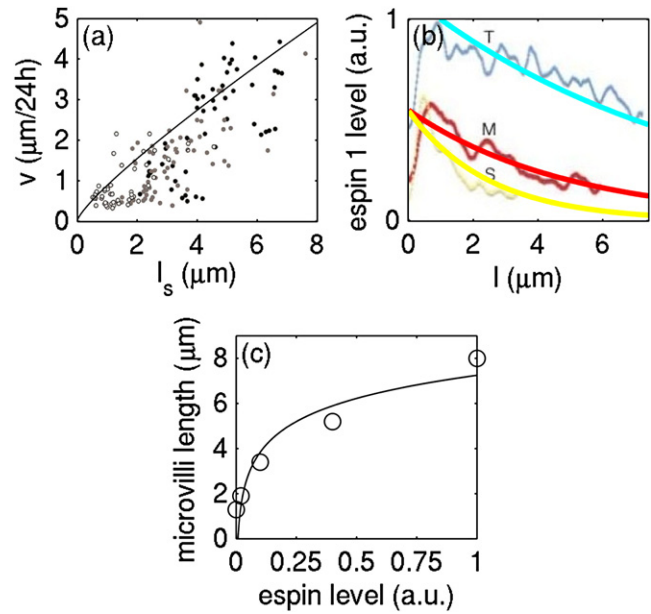


FIGURE 2 Dependence of the protrusion length on various parameters predicted by Eq. 6 and determined from experiments. (a) Measured treadmilling velocity versus length in the stereocilia of the rat cochlea. In mammals, cochlear stereocilia are arranged into three rows of graded height (black circles, experimental data for the tallest row; gray circles, middle row; and open circles, shortest row). (Line) Plot of Eq. 6, using the same value $k_{\text{off}} = 0.14 \text{ h}^{-1}$ as in Fig. 1 b. Experimental data taken from Rzadzinska et al. (5). (b) Espin 1 density as a function of ℓ in the vestibular stereocilia of guinea pigs. The three curves correspond to three stereocilia of the same hair cell with different lengths ($T \approx 35 \mu\text{m}$, $M \approx 20 \mu\text{m}$, and $S \approx 10 \mu\text{m}$). Agreement with Eq. 1 is found for $k_{\text{off}} = 0.35 \text{ h}^{-1}$, which is of the same order of magnitude as the value deduced from the fit of Fig. 1 b. Experimental data taken from Salles et al. (24). (c) Dependence of microvilli length in CL4 cells on the espin overexpression level. Experimental data taken from Loomis et al. (15).

average elongation is measured and correlated to the espin expression level. Assuming that espin is incorporated at the tip of the protrusion at a rate proportional to its expression level c_e , we can consider that P_0 is proportional to c_e . Following this, Eq. 6 yields a prediction for the dependence of ℓ_s on c_e , which we show in Fig. 2 c. We use two new adjustable parameters there, as these experiments deal with a different cell type and with other protrusions than stereocilia (in particular, the renewal time of microvilli is much shorter than that of stereocilia). The best fit is found for $v/k_{\text{off}} = 1.5 \mu\text{m}$. The value of the other parameter,

$$d\left(\frac{nvP_0}{ak_{\text{off}}}\right) / dc_e,$$

does not contain any exploitable information because only relative values of c_e are known experimentally.

Overall, we find that the simple case where espin does not reattach to actin yields good agreement with experimental data, while relying on only one adjustable parameter. Note also that the stereocilium length given by Eq. 6 has a smooth dependence on both v/k_{off} and nvP_0/ak_{off} , as illustrated by

Fig. 2, *a* and *c*. This makes the stereocilium robust with respect to perturbations of the cellular conditions, which is expected for such a well-regulated structure.

SINGLE FILAMENT WITH REATTACHMENT

Although the results presented above give a good description of the shape of experimentally observed stereocilia, it is interesting to study the effects of espin reattachment in our model. We might indeed have to take this effect into account in more detailed studies of stereocilia or when interested in other types of cellular protrusions. In such protrusions, cross-linkers detaching from the actin filaments might diffuse for a while, and then reattach elsewhere in the actin bundle. If diffusion is considered fast in the sense of Model for the Actin and Cross-Linker Dynamics, this is equivalent to putting the filament in contact with a reservoir of cross-linkers, represented by the attachment rate k . In this configuration, the espin dynamics influences actin depolymerization in the same way as above, but unlike in Stereocilium Shape without Espin Reattachment, actin depolymerization now also influences the espin dynamics. Indeed, espin can reattach at a given site only if this site is surrounded by two actin filaments. Therefore, in contrast to the previous section, actin is no longer slaved to espin.

In this section, we consider only the simplified case of a single filament cross-linked to a wall, as shown in Fig. 3 *a*. We furthermore assume that $P_0 = 1$, i.e., that the actin bundle is completely cross-linked at the polymerization front. In Discrete Master Equation and Solution Far from the Polymerization Front, we write a master equation for the dynamics of the filament's depolymerizing end and solve it far from the polymerization front. We then consider the case where the depolymerizing end comes close to the polymerization front and discuss the resulting treadmilling steady state in Growth Transition and Stationary State.

Discrete master equation and solution far from the polymerization front

Unlike in the previous section, in the following we consider the altitude in the reference frame of the filament, not of the polymerization front. We assume that the polymerization front is at altitude zero at time $t = 0$. Because it moves with a velocity v in the reference frame of the filament, it is at altitude vt at time t . Thus the altitude $z = vt - \ell$ of the pointed end of the filament is an integer smaller than or equal to the altitude vt of the polymerization front (Fig. 3 *a*).

Let us define the quantity

$$\delta(i, t) = \exp \left[- (1 + k) \left(t - \frac{i}{v} \right) \right]. \quad (7)$$

In Sec. S2.1 in the Supporting Material, we write a master equation for the model described in Model for the Actin

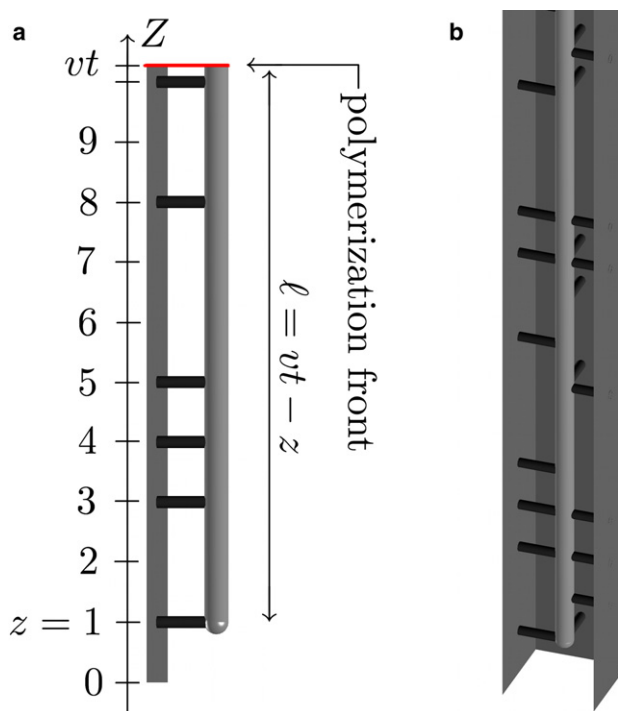


FIGURE 3 Schematics of the single-filament problem. (a) Single filament bound to a single wall and the coordinate system used in Single Filament with Reattachment. (b) Single filament bound to $n = 3$ walls.

and Cross-Linker Dynamics and show that the probability $P(Z, t)$ for the filament's depolymerizing end to be at altitude Z such that $0 \leq Z < vt$ at time t obeys the simplified master equation

$$\begin{aligned} \partial_t P(Z, t) = & -P(Z, t) + \frac{k + \delta(Z, t)}{1 + k} \\ & \times \sum_{Z'=-\infty}^{Z-1} \left[\prod_{i=Z'+1}^{Z-1} \frac{1 - \delta(i, t)}{1 + k} \right] P(Z', t), \end{aligned} \quad (8)$$

with the boundary condition at the polymerization front

$$\partial_t P(\lfloor vt \rfloor, t) = \sum_{Z'=-\infty}^{\lfloor vt \rfloor - 1} \left[\prod_{i=Z'+1}^{\lfloor vt \rfloor - 1} \frac{1 - \delta(i, t)}{1 + k} \right] P(Z', t), \quad (9)$$

and where we assume that the filament has a vanishing length at $t = 0$:

$$P(Z, t = 0) = \delta_{Z,0}. \quad (10)$$

Here $\lfloor x \rfloor$ denotes the integral part (or floor) of real number x , and $\delta_{i,j}$ is the Kronecker delta. Note that the probability distribution from Eq. 3 is a solution of this problem in the special case $n = 1$, $k = 0$, $P_0 = 1$ (see Sec. S2.2 in the Supporting Material).

We now consider the altitude i located strictly above the depolymerizing end of the filament and strictly below the polymerization front (i.e., $Z < i < vt$). We show in Sec. S2.1.3 in the Supporting Material that the probability for the espin site located at altitude i to be occupied is

$$\frac{k + \delta(i, t)}{1 + k}$$

The function $\delta(i, t)$ can thus be interpreted as the deviation of the espin density at site i from the steady-state density $k/(1+k)$ corresponding to a situation where site i is in equilibrium with the espin reservoir. This imbalance originates in the fact that espin sites are always occupied at the polymerization front (they are incorporated into the actin bundle with a probability of 1). With time, however, espin sites lose the memory of their initial conditions, and relax back to an equilibrium with the espin reservoir. This is reflected by the fact that $\delta(i, t)$ vanishes far away from the polymerization front, i.e., in the region where $vt - i \gg v/(1+k)$. Let us assume that the filament's depolymerizing end is at the altitude

$$\bar{z} \gg \frac{v}{1+k}$$

at time \bar{t} . We solve this problem exactly in Sec. S2.3 in the [Supporting Material](#). We then show that on long timescales the dynamics of the depolymerizing end is well approximated by the Gaussian distribution

$$P(Z, t) \underset{t \rightarrow +\infty}{\propto} \exp \left\{ -\frac{k^2}{2(1+k)(2+k)(t-\bar{t})} \times \left[Z - \bar{z} - \frac{(1+k)(t-\bar{t})}{k} \right]^2 \right\}. \quad (11)$$

This is characteristic of a biased diffusion with diffusion coefficient

$$D_d = \frac{(1+k)(2+k)}{2k^2}$$

and average depolymerization velocity

$$v_d = \frac{1+k}{k}.$$

The depolymerization velocity can be recovered from the following very simple argument: consider a filament cross-linked to the wall at its pointed end. Because the cross-link detaches with a rate 1, the average waiting time for the filament to unpin is $\tau = 1$. Once the filament is released, it quickly depolymerizes to the next cross-linker, and then becomes pinned again. Because the espins are at equilibrium with the reservoir, the average cross-linker density is

$$\rho = \frac{k}{1+k},$$

meaning that the filament depolymerizes over an average distance $d = 1/\rho$ before becoming pinned again. Therefore, the average depolymerization velocity of the filament is

$$v_d = d/\tau = \frac{1+k}{k}.$$

Growth transition and stationary state

If the depolymerization velocity v_d is smaller than the polymerization velocity ($v_d < v$), then the pointed end never catches up on the polymerization front, and [Eq. 11](#) is a good approximation of its dynamics. In this case, the filament length—which is equal to the distance between polymerization front and pointed end—grows indefinitely at velocity $v - v_d$ and the filament has no stationary state. Heavy cross-linking of the actin favors this regime, because it has the effect of slowing depolymerization down. However, v_d cannot be smaller than 1, which corresponds to a maximally cross-linked situation (i.e., to jumps of size 1 at a rate 1). Therefore, if $v < 1$, the growth regime described here does not exist. Conversely, if the depolymerization velocity is larger than the polymerization velocity ($v_d > v$), the pointed end moves closer and closer to the polymerization front. Thus, the length of the filament is bounded in this regime. This is the situation considered in this section.

We hereafter call the threshold $v = v_d$ the growth transition. As it comes closer to the polymerization front, the pointed end penetrates into regions where the cross-links have not yet lost the memory of their incorporation into the bundle, and are therefore denser than at equilibrium. More specifically, their average density is given by

$$\rho(\ell) = \frac{k + e^{-\frac{1+k}{v}\ell}}{1+k}, \quad (12)$$

where $\ell = vt - z$ is the length of the filament. Using the same argument as in the previous section, the depolymerization velocity of a filament of length ℓ is equal to $1/\rho(\ell)$. A stationary filament length is obtained when this velocity matches the polymerization velocity. This reasoning yields an estimate for the stationary length ℓ_s ,

$$v = \frac{1}{\rho(\ell_s)} \Leftrightarrow \ell_s = \frac{v}{1+k} \ln \left[\frac{1}{(1+k) \left(\frac{1}{v} - \frac{1}{v_d} \right)} \right], \quad (13)$$

where

$$v_d = \frac{1+k}{k}.$$

[Equation 13](#) matches [Eq. 6](#) for $k = 0$, $P_0 = 1$, and $n = 1$. In vivo, stereocilia are much longer than the spacing between two cross-linkers, meaning that we are interested in the regime $\ell_s \gg 1$. There are two ways to enter this regime. One is for the logarithm in [Eq. 13](#) to be very large, which can only be achieved if

$$\frac{1}{v} - \frac{1}{v_d} \ll 1.$$

This happens when the polymerization and equilibrium depolymerization velocities are very well matched. Because we expect the stereocilium shape to be robust under

perturbations of the model parameters, this is not reasonable from a biological point of view. Therefore, we discard this first way of obtaining $\ell_s \gg 1$ and turn to the second one, which is

$$\frac{v}{1+k} \gg 1.$$

In this case, because $v < v_d$,

$$1 \ll \frac{v}{1+k} < \frac{v_d}{1+k} = \frac{1}{k}. \quad (14)$$

This implies $k \ll 1$, meaning that we do not need to consider the depolymerization problem in all its generality, but only its small- k , large- v limit. Let $\alpha = kv$. Multiplying Eq. 14 by k , we note that below the growth transition, $0 \leq \alpha < 1$. Therefore, in the limit of large v , the growth transition occurs for $\alpha = 1$ (or equivalently $v = v_d = (1+k)/k$, which is its definition). The interesting regimes to consider are therefore those where α is of order 1, and in the following we take the $v \rightarrow +\infty$ limit at fixed, finite α .

In Sec. S3.2 in the [Supporting Material](#), we generalize our approach to a filament bound to a number n of walls, as exemplified in Fig. 3 b. Defining the coordinate ξ by

$$\ell = vt - Z = v \ln v + v\xi, \quad (15)$$

we expect from Eq. 13 that the interesting part of the dynamics takes place in the scaling region $\xi \approx 1$. Indeed, we show in Sec. S3.3 in the [Supporting Material](#) that the master equation has the following continuum limit:

$$\begin{aligned} \frac{dP}{d\xi}(\xi) &= -P(\xi) + n(\alpha + e^{-\xi}) \exp(n\alpha\xi - ne^{-\xi}) \\ &\times \int_{\xi}^{+\infty} \frac{P(\xi')}{\exp(n\alpha\xi' - ne^{-\xi'})} d\xi'. \end{aligned} \quad (16)$$

The stationary profile of the filament length probability distribution is the only normalized stationary solution of this equation. The corresponding cumulative distribution reads (see Sec. S3.4 in the [Supporting Material](#))

$$P^{\leq}(\xi) = \frac{\Gamma(1 - n\alpha, ne^{-\xi})}{\Gamma(1 - n\alpha)}. \quad (17)$$

Here $\Gamma(b) = \Gamma(b, 0)$ is the usual γ -function, where the incomplete γ -function is defined as

$$\Gamma(b, x) = \int_x^{+\infty} (u^{b-1} e^{-u}) du. \quad (18)$$

Plots of P^{\leq} as a function of ℓ are presented in Fig. 5. Equation 17 implies that the average filament length diverges as

$$\langle \ell \rangle \underset{k \rightarrow k_c^-}{\sim} \frac{v}{1 - nk v} \propto \frac{1}{|k - k_c|}, \quad (19)$$

when k approaches the critical value

$$k_c = \frac{1}{nv}. \quad (20)$$

Therefore, for a large enough espin reattachment rate, a stationary filament profile ceases to exist. This is the n -walls generalization of the growth transition discussed at the beginning of this section. Indeed, for $k \geq k_c$, espin slows the depolymerization down so much that the pointed end can never catch up on the polymerization front.

COUPLING BETWEEN FILAMENTS

In this section we use Monte Carlo simulations of a square ($n = 4$) lattice of filaments (described in Sec. S4.1 in the [Supporting Material](#)) to study the effect of espin reattachment in the biologically relevant situation of a stereocilium composed of several filaments. In the following, we focus on long stereocilia, for which we expect the continuum approach introduced in Growth Transition and Stationary State to apply. This approach is valid for $v \gg 1$. Because simulating long bundles is time-consuming, we use $v = 20$ throughout, which represents a good compromise. Unlike in the previous section, filaments are bound to each other and not to walls. Their espin environment thus depends on both their altitude and on the state of their neighbors. In the next subsection, we study how this modifies the growth transition. Then, in the following subsection, Multifilament Stereocilium Profiles, we compare the stereocilium shapes obtained from numerical simulations to those derived from a one-filament calculation.

Couplings modify the growth transition

To investigate whether multifilament bundles have a growth transition, we simulate several 8×8 periodic filament bundles for various value of the espin reattachment rate k .

We first focus on the values of k where stationary stereocilium profiles exist and monitor the average filament length, as shown in Fig. 4 a. At $k = k_c = 0.02$, the average filament length diverges, showing that coupled filaments do undergo a growth transition. This value of k_c matches the threshold of Eq. 20 if n is set to $n^{\text{eff}} = 2.5$. This effective n can approximately be viewed as the average number of neighbors available for each filament to cross-link at each given instant, i.e., the number of neighbors as long as or longer than the filament. We give an argument for its numerical value in Sec. S4.2 in the [Supporting Material](#). In Fig. 4 a, we fit a power law to the divergence of the stereocilium length and show that

$$\langle \ell \rangle \underset{k \rightarrow k_c^-}{\propto} \frac{1}{|k - k_c|^{0.33}}, \quad (21)$$

which is an anomalous divergence compared to the case of Eq. 19. This is likely to be related to the build-up of

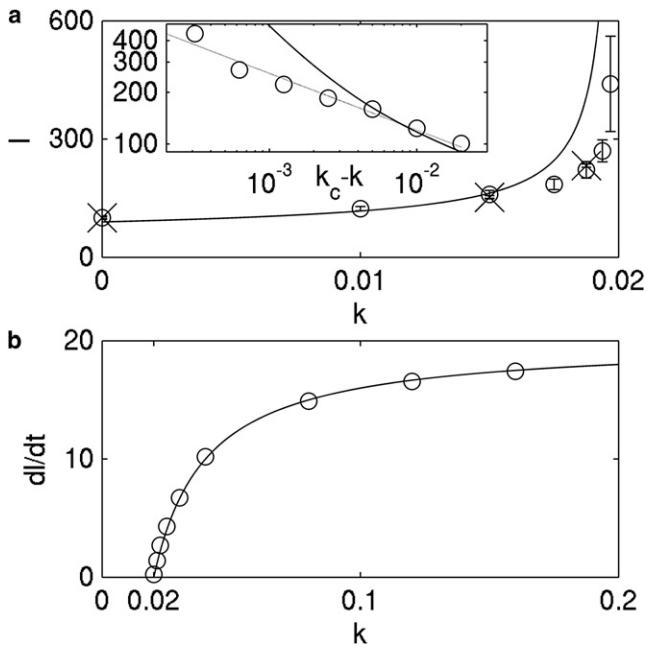


FIGURE 4 Growth transition for multifilament bundles with reattachment. (a) Average length as a function of k below the transition and comparison with the average length calculated from Eq. 17 for $n = 2.5$ (line). (Open circles) 8×8 periodic arrays. (Crosses) 16×16 periodic arrays, showing that the lengths do not depend much on the simulation size. Error bars represent the root-mean-square height fluctuations in the steady state. (Inset) Log-log representation of the same $\langle \ell \rangle$ data from 8×8 arrays as a function of the distance $k_c - k$ to the growth transition threshold. (Solid line) Prediction from Eq. 17 as in the main figure. (Dotted line) Power law fit as in Eq. 21. (b) Growth velocity of the bundle as a function of k above the growth transition for 8×8 periodic arrays (open circles) and comparison to the generalization of the one-filament theory given in Eqs. 22 and 23 for $n = 2.5$ (line).

long-ranged correlations across the actin bundle, as discussed in Sec. S4.3 in the Supporting Material.

For values of k above the growth transition, the stereocilium grows indefinitely and at constant velocity. In Fig. 4 b, we plot the stereocilium's growth velocity as a function of k . As k is reduced, the pointed ends depolymerize faster and faster and catch up to the polymerization front for $k_c = 0.02$, which is consistent with the threshold determined in Fig. 4 a. At steady state, the stereocilium lengthening velocity is the difference between its polymerization velocity and its depolymerization velocity far from the polymerization front:

$$\frac{d\ell}{dt} = v - v_d. \quad (22)$$

This growth velocity vanishes at the growth transition. While v is imposed in our simulations, v_d depends on k and n . We now discuss our theoretical predictions for this dependence. Far away from the polymerization front, the probability for an espn to be on is $k/(1+k)$. In the cases considered here, $k \ll 1$, meaning that espns are scarce far from the polymerization front: the probability for a given pointed end to be bound to more than one cross-linker is

negligible. Thus, the interesting part of the filament is bound to cross-linkers with an average density ρ , and is very unlikely to be bound to more than one cross-linker at any given altitude. The discussion at the end of Discrete Master Equation and Solution Far From the Polymerization Front thus applies, although the density of the cross-linkers in the case considered here is n times larger, because there are n walls instead of one. To lowest order in k , this yields

$$v_d = \frac{1}{nk}. \quad (23)$$

This single-filament result is compared to the multifilament simulations in Fig. 4 b using $n = n^{\text{eff}}$, and the two are found to be in very good agreement. Note that we expect the function $v_d(k)$ to diverge as k goes to 0, but to be a smooth function of k for $k > 0$. In particular, $v_d(k)$ has no reason to have a singularity in $k = k_c$: indeed, k_c is defined by $v_d(k_c) = v$, and v_d does not depend on v . Thus, $k = k_c$ is a generic point of the function $v_d(k)$. Therefore, at the transition, the following generic crossing scenario applies, whether or not the filaments are coupled:

$$\frac{d\ell}{dt}(k) \underset{k \rightarrow k_c^+}{\propto} (k - k_c). \quad (24)$$

Multifilament stereocilium profiles

We now return to the question of the shape of stereocilia. In Fig. 5, we compare the shapes obtained from the simulations with theoretical expectations from the single-filament theory. For each value of k , the theoretical curve Eq. 17 is plotted using the effective number of neighbors $n^{\text{eff}} = 2.5$ from the previous subsection. As k is increased, the description of the bundle by the single-filament theory becomes worse and worse, as expected from Fig. 4 a.

Another theoretical result our simulations should be compared with is Eq. 17 using the actual number of neighbors $n = 4$. Note, however, that this is only possible for k smaller than 0.0125, which is the growth transition threshold for $n = 4$. Consistent with this, we plot the $n = 4$ theoretical curve only in Fig. 5 a, where $k = 0$. Excellent agreement with the numerical simulations is found. This is expected, because when espns are not allowed to reattach, Eq. 17 is identical to Eq. 5—which is the exact solution of the multifilament problem for $k = 0$.

In Fig. 5 b, we illustrate the dependence of the bundle shape on the number of filaments included in the simulations. No change in the shape is observed when multiplying the number of filaments by four, but the amplitude of the fluctuations is reduced. This suggests that in this regime at least, the average profile given by our 8×8 simulations is a good assessment of the infinite bundle limit.

In Fig. 5 c, we illustrate the dependence of the bundle shape on the boundary conditions of the bundle. It is found that a circular bundle (see illustration in Fig. S3 a in Supporting Material) is markedly shorter than a bundle with

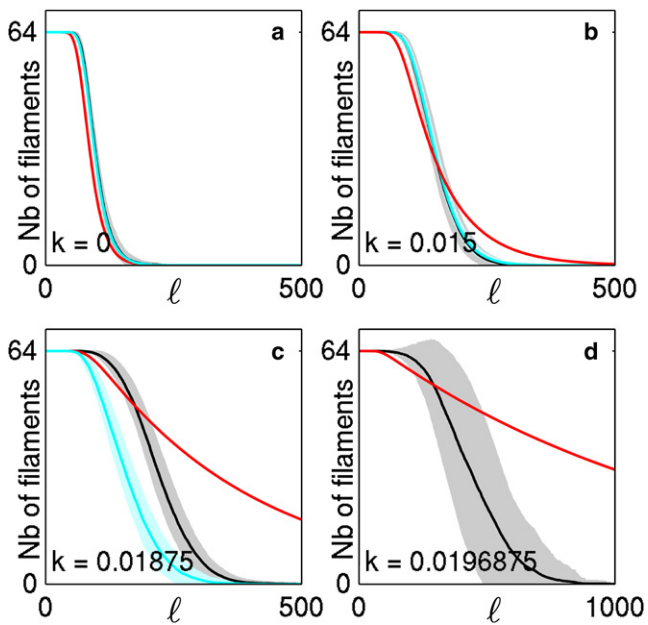


FIGURE 5 (Color online) Profiles of multifilament bundles for various values of k . (Red lines; leftmost line in (a) and rightmost line in (b-d)) $P^> = 1 - P^{\leq}$, with P^{\leq} given by the single-filament theory equation (Eq. 17) scaled to the number of filaments in the bundle with $n = 2.5$. (Black lines) Average number of filaments longer than ℓ for numerical 8×8 bundles. (Gray area) Standard deviation of the steady-state fluctuations around this average. The cyan (gray) lines have different meanings depending on the figure considered. (a) $n = 4$ single filament theory, equivalent to the fit of Fig. 1 b; note that the representation used here does not reflect the aspect ratio of the predicted stereocilia shapes. (b) Average number of filaments longer than ℓ and fluctuations for a 16×16 bundle (data normalized to match the black line in $\ell = 0$). (c) Average number of filaments longer than ℓ and fluctuations for a circular bundle of 32 filaments (data normalized to match the black line in $\ell = 0$). Note the contracted ℓ scale in panel d, as compared to panels a–c.

periodic boundary conditions. This is because the filaments close to the rim of the circular bundle tend to depolymerize faster, due to the fact that they have fewer neighbors. In the parameter regime presented here, this is sufficient to reduce the average length of the bundle significantly. This effect becomes negligible for small k and for large bundle radii, i.e., if the filaments are correlated over a length much shorter than the radius of the bundle.

Finally, in Fig. 5 d we note that as the growth transition is approached, the amplitude of the bundle's fluctuations increases dramatically. Indeed, as the depolymerization velocity becomes very close to the polymerization velocity, the filaments are more and more loosely confined to a finite length. Similarly to what happens, e.g., for a Brownian particle in a harmonic potential, a looser confinement leads to fluctuations of a larger amplitude.

DISCUSSION

In this article we present a simple physical model for the morphogenesis of stereocilia, whose very well-regulated

shapes are crucial for the frequency selectivity of hearing in a wide range of animals. Our model is to be understood in the framework of Prost et al. (8), where the shape of stereocilia is attributed to an “internal clock” of the actin bundle. Here we propose that the internal clock is provided by the stochastic attachment-detachment dynamics of the well-characterized protein espin, or some other actin cross-linker.

Although the emphasis of this article is on stereocilia, the simplicity of our model makes it general enough to describe several other biological length-regulation processes (28). The most obvious of these are of course other cellular protrusions, such as filopodia, microvilli, and *Drosophila* bristles, where actin filaments are also coupled by cross-linkers. More specifically, in filopodia the ratio of the actin treadmilling velocity (29) and detachment rate of the cross-linker fascin (30) is $\approx (1 \mu\text{m}/\text{min})/(0.12 \text{ s}^{-1}) \approx 1 \mu\text{m}$, which is commensurate with the length of this type of protrusion. This suggests that the mechanism described here could be relevant in filopodia. In addition, the study presented in Single Filament with Reattachment is relevant to single-filament problems where each monomer stochastically switches between two states, such as the phosphorylation-dependent depolymerization of a single actin filament (16) or microtubule (31), or association with proteins making the filament more susceptible to depolymerization (32).

Stereocilia models have been previously proposed in the literature that yield good agreement with electron micrographs of stereocilia. This article is based on Prost et al. (8), which analyzes the forces at play in stereocilium treadmilling and the interaction of the actin bundle with the membrane and the cytoplasm. Here we improve on this work by proposing a refined description of the dynamics of the actin bundle itself based on the role of cross-linkers. This leads to improvements in three directions, which evidences the importance of espin in shaping stereocilia:

First, the model of Prost et al. (8) depends partly on a hypothetical actin pointed end-capping protein, whereas we only assume well-identified proteins. Note that Prost et al. (8) suggests that espin could be described as such a capping protein. We show here, however, that there are important differences:

1. Our model cross-links interact with the actin all along the filament, whereas capping proteins only bind to its end.
2. The probability for the pointed end to be cross-linked depends on the filament length.
3. Capping proteins introduce no interfilament correlations.

Second, the stereocilia shapes calculated in Prost et al. (8) resemble those of deaf *Shaker 2J* mutants, while we account for those of healthy animals.

Third, the shapes of Prost et al. (8) are highly sensitive on the fine tuning of actin's polymerization and depolymerization rates, which is not compatible with the biological robustness of the well-controlled stereocilia shapes.

Another quite different model is proposed in Naoz et al. (7). It is based on the fact that actin-associated proteins could be actively localized at the stereocilium base, e.g., by molecular motors. For instance, this work suggests that actin-severing proteins localized at its base could drive the narrowing of the actin bundle there. This model offers an interesting insight into the possible roles of the experimentally observed active transport within the stereocilium. It is, however, difficult to assess its validity quantitatively, because it hypothesizes several experimentally uncharacterized protein-protein interactions, and has an accordingly large number of adjustable parameters. Note also that this model does not address the issue of the stereocilium height regulation.

The model presented in this article is in agreement with several experiments showing the importance of espin in stereocilium length regulation. We predict that the actin bundle can only reach a stationary profile if the attachment rate of espin to actin is much smaller than its detachment rate ($k \approx v^{-1} \ll 1$). This is consistent with the observation made in Rzadzinska et al. (5) that espin in the stereocilium seems to treadmill along with actin—in other words, that espin is essentially incorporated at the tip of the stereocilium and not so much exchanged with the solution in the bulk of the actin bundle. More quantitatively, we are able to reproduce the shape of several stereocilia within the same hair bundle with only one adjustable parameter. We also account for the apparent proportionality between stereocilium length and turnover time, as well as for espin 1 localization at the stereocilium tip. Finally, our approach faithfully captures the quantitatively measured relationship between microvillus length and espin expression. A possible extension of our model as applied to stereocilia would be to consider that the espin detachment dynamics might be different in the bulk of the actin bundle and at its lateral surface. For instance, in the presence of preferential espin detachment at the surface, actin filament termination would happen more rarely in the bulk. This could account for the fact that filament bending as pictured in Fig. S1 in the Supporting Material is not clearly observed in electron micrographs.

On a broader level, the dynamics of the cytoskeleton involves many out-of-equilibrium surface growth processes. In addition to actin bundle-based protrusions, one could quote the dynamics of the cell cortex, which undergoes polymerization and depolymerization as well as transient cross-linking, similarly to the system studied here. In addition, its dynamics involves actin filament branching and barbed end capping, as well as molecular motors binding which makes it contractile. Another similarly complicated system is the lamellipodium, a thin sheet of actin that some cell types (e.g., keratocytes) extend in front of them while moving.

The precise interplay between all the sources of activity in these processes is not well understood. The more formal aspects of our study of the novel, nontrivial growth model introduced here reveal interesting directions to pursue in order to characterize those processes. Indeed, in the sections

Single Filament with Reattachment and Coupling between Filaments, we discuss what we expect to be two very robust features that might be universal across a large range of cross-linking-limited disassembly models: the growth transition and an anomalous length divergence exponent in the presence of local interactions between filaments. By identifying those features and recognizing them in actual cellular systems, one might be able to use them as signatures of the underlying interface-shaping phenomena, and therefore show which mechanism dominates which type of interface.

SUPPORTING MATERIAL

Four figures and 72 equations are available at [http://www.biophysj.org/biophysj/supplemental/S0006-3495\(10\)00974-4](http://www.biophysj.org/biophysj/supplemental/S0006-3495(10)00974-4).

We thank Pascal Martin for stimulating discussions.

REFERENCES

1. Lin, H. W., M. E. Schneider, and B. Kachar. 2005. When size matters: the dynamic regulation of stereocilia lengths. *Curr. Opin. Cell Biol.* 17:55–61.
2. Holmes, K. C., D. Popp, ..., W. Kabsch. 1990. Atomic model of the actin filament. *Nature.* 347:44–49.
3. Manor, U., and B. Kachar. 2008. Dynamic length regulation of sensory stereocilia. *Semin. Cell Dev. Biol.* 19:502–510.
4. Schneider, M. E., I. A. Belyantseva, ..., B. Kachar. 2002. Rapid renewal of auditory hair bundles. *Nature.* 418:837–838.
5. Rzadzinska, A. K., M. E. Schneider, ..., B. Kachar. 2004. An actin molecular treadmill and myosins maintain stereocilia functional architecture and self-renewal. *J. Cell Biol.* 164:887–897.
6. Sakaguchi, H., J. Tokita, ..., B. Kachar. 2008. Dynamic compartmentalization of protein tyrosine phosphatase receptor Q at the proximal end of stereocilia: implication of myosin VI-based transport. *Cell Motil. Cytoskeleton.* 65:528–538.
7. Naoz, M., U. Manor, ..., N. S. Gov. 2008. Protein localization by actin treadmill and molecular motors regulates stereocilia shape and treadmill rate. *Biophys. J.* 95:5706–5718.
8. Prost, J., C. Barbetta, and J.-F. Joanny. 2007. Dynamical control of the shape and size of stereocilia and microvilli. *Biophys. J.* 93:1124–1133.
9. Itoh, M. 1982. Preservation and visualization of actin-containing filaments in the apical zone of cochlear sensory cells. *Hear. Res.* 6:277–289.
10. Tilney, L. G., E. H. Egelman, ..., J. C. Saunders. 1983. Actin filaments, stereocilia, and hair cells of the bird cochlea. II. Packing of actin filaments in the stereocilia and in the cuticular plate and what happens to the organization when the stereocilia are bent. *J. Cell Biol.* 96:822–834.
11. Tilney, M. S., L. G. Tilney, ..., A. Bretschner. 1989. Preliminary biochemical characterization of the stereocilia and cuticular plate of hair cells of the chick cochlea. *J. Cell Biol.* 109:1711–1723.
12. Zheng, L., G. Sekerková, ..., J. R. Bartles. 2000. The deaf jerker mouse has a mutation in the gene encoding the espin actin-bundling proteins of hair cell stereocilia and lacks espins. *Cell.* 102:377–385.
13. Sekerková, G., L. Zheng, ..., J. R. Bartles. 2006. Espins and the actin cytoskeleton of hair cell stereocilia and sensory cell microvilli. *Cell. Mol. Life Sci.* 63:2329–2341.
14. Chen, B., A. Li, ..., J. R. Bartles. 1999. Espin contains an additional actin-binding site in its N terminus and is a major actin-bundling protein of the Sertoli cell-spermatid ectoplasmic specialization junctional plaque. *Mol. Biol. Cell.* 10:4327–4339.

15. Loomis, P. A., L. Zheng, ..., J. R. Bartles. 2003. Espin cross-links cause the elongation of microvillus-type parallel actin bundles in vivo. *J. Cell Biol.* 163:1045–1055.
16. Fujiwara, I., S. Takahashi, ..., S. Ishiwata. 2002. Microscopic analysis of polymerization dynamics with individual actin filaments. *Nat. Cell Biol.* 4:666–673.
17. Donaudy, F., L. Zheng, ..., P. Gasparini. 2006. Espin gene (ESPN) mutations associated with autosomal dominant hearing loss cause defects in microvillar elongation or organization. *J. Med. Genet.* 43:157–161.
18. Tilney, L. G., P. S. Connelly, ..., G. M. Guild. 2003. Actin filament turnover regulated by cross-linking accounts for the size, shape, location, and number of actin bundles in *Drosophila* bristles. *Mol. Biol. Cell.* 14:3953–3966.
19. Rzadzinska, A., M. Schneider, ..., B. Kachar. 2005. Balanced levels of Espin are critical for stereociliary growth and length maintenance. *Cell Motil. Cytoskeleton.* 62:157–165.
20. Li, H., H. Liu, ..., S. Heller. 2004. Correlation of expression of the actin filament-bundling protein espin with stereociliary bundle formation in the developing inner ear. *J. Comp. Neurol.* 468:125–134.
21. Sekerková, G., L. Zheng, ..., J. R. Bartles. 2006. Differential expression of espin isoforms during epithelial morphogenesis, stereociliogenesis and postnatal maturation in the developing inner ear. *Dev. Biol.* 291:83–95.
22. Mogensen, M. M., A. Rzadzinska, and K. P. Steel. 2007. The deaf mouse mutant whirler suggests a role for whirlin in actin filament dynamics and stereocilia development. *Cell Motil. Cytoskeleton.* 64:496–508.
23. Belyantseva, I. A., E. T. Boger, ..., T. B. Friedman. 2005. Myosin-XVa is required for tip localization of whirlin and differential elongation of hair-cell stereocilia. *Nat. Cell Biol.* 7:148–156.
24. Salles, F. T., R. C. J. Merritt, Jr., ..., B. Kachar. 2009. Myosin IIIa boosts elongation of stereocilia by transporting espin 1 to the plus ends of actin filaments. *Nat. Cell Biol.* 11:443–450.
25. Fettiplace, R., and C. M. Hackney. 2006. The sensory and motor roles of auditory hair cells. *Nat. Rev. Neurosci.* 7:19–29.
26. Bartles, J. R., L. Zheng, ..., B. Chen. 1998. Small espin: a third actin-bundling protein and potential forked protein ortholog in brush border microvilli. *J. Cell Biol.* 143:107–119.
27. Haviv, L., N. Gov, ..., A. Bernheim-Groswasser. 2008. Thickness distribution of actin bundles in vitro. *Eur. Biophys. J.* 37:447–454.
28. Daniels, D. R. 2010. Effect of capping protein on a growing filopodium. *Biophys. J.* 98:1139–1148.
29. Mallavarapu, A., and T. Mitchison. 1999. Regulated actin cytoskeleton assembly at filopodium tips controls their extension and retraction. *J. Cell Biol.* 146:1097–1106.
30. Aratyn, Y. S., T. E. Schaus, ..., G. G. Borisy. 2007. Intrinsic dynamic behavior of fascin in filopodia. *Mol. Biol. Cell.* 18:3928–3940.
31. Dimitrov, A., M. Quesnoit, ..., F. Perez. 2008. Detection of GTP-tubulin conformation in vivo reveals a role for GTP remnants in microtubule rescues. *Science.* 322:1353–1356.
32. Varga, V., J. Helenius, ..., J. Howard. 2006. Yeast kinesin-8 depolymerizes microtubules in a length-dependent manner. *Nat. Cell Biol.* 8:957–962.

Biophysical Journal, Volume 99

Supporting Material

Actin cross-linkers and the shape of stereocilia

Martin Lenz, Jacques Prost, and Jean-François Joanny

Keywords: Actin depolymerization; Espin; Growth process; Interacting filaments

Actin Cross-Linkers and the Shape of Stereocilia

Supporting Material

S1 Membrane tension pushes the filaments together

Here we present numerical estimates in support of the notion that the membrane tension pushes the sparse actin filaments represented in Fig. 1(a) of the main text into a dense bundle, as pictured in Fig. S1.

As a consequence of the model described in the section Model for the Actin and Cross-Linker Dynamics of the main text, we expect the lower end of the actin bundle to have a very irregular shape due to the stochastic character of the espin detachment and subsequent actin depolymerization [Fig. 1(a)]. At first sight, this does not seem consistent with the smooth tapered ends observed experimentally (1). The two behaviors are however compatible if one takes into account the influence of the membrane. Indeed, as the radius of the stereocilium ($\simeq 200$ nm) is larger than the natural membrane tether radius $[(\kappa/2\sigma)^{1/2} \simeq \text{a few tens of nm}]$ (2), the dominant influence of the membrane is that of its tension σ , which tends to compress the tube and therefore push the irregularly distributed filaments together, as illustrated in Fig. S1. In doing so, the membrane lowers its surface tension energy by an amount $\approx \sigma \ell_t \delta r_t$, and a number ≈ 100 of actin filaments are bent with a radius of curvature $\approx \ell_t^2 / \delta r_t$ over a length $\approx \ell_t$, hence a cost $\approx 100 k_B T \ell_p \times \ell_t \times (\delta r_t / \ell_t^2)^2$ in bending energy, where ℓ_p is the persistence length of actin and the other lengths are defined in Fig. S1. Using $\sigma \simeq 10^{-5} \text{ N.m}^{-1}$, $\ell_t \simeq 10 \mu\text{m}$, $\delta r_t \simeq 100 \text{ nm}$ and $\ell_p \simeq 10 \mu\text{m}$, we find that the tension energy gain $\approx 10^{-17} \text{ J}$ upon pushing the filaments into a tapered shape exceeds the filament bending energy cost $\approx 4 \times 10^{-23} \text{ J}$ by far, thus validating our picture. Indeed, experimentally, actin filaments are observed to be packed together throughout the stereocilium (3). Because of this packing mechanism, actin filaments that are not neighbors in $\ell = 0$ might come into contact. Here we neglect the possibility that such accidental neighbors become cross-linked by espin. Therefore, we take into account the spatial structure of the bundle in the horizontal direction only through the notion of nearest neighbor in the initial ($\ell = 0$) paracrystal.

Since espin is in principle able to bind the membrane (4) and it has been shown experimentally that cross-linkers-mediated contact with the membrane stabilizes actin bundles during *Drosophila* bristle disassembly (5), the membrane surrounding the actin bundle might to some extent be able to stabilize an actin filament through cross-linking in a similar way that a neighboring filament does. The question of the influence of the lateral boundary conditions on the stereocilium shape is further discussed in the section Multi-Filament Stereocilium Profiles.

S2 Single-filament dynamics with reattachment

Here we give the details of the calculations presented in the section Discrete Master Equation and Solution Far from the Polymerization Front.

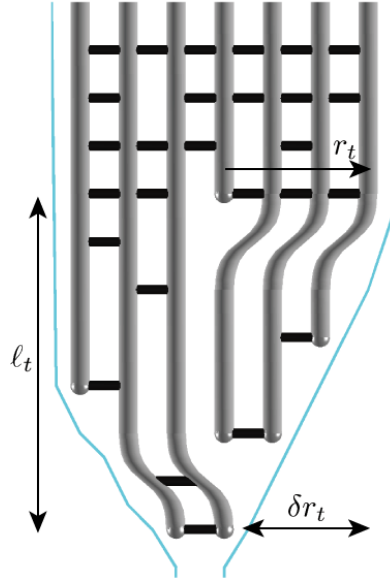


Figure S1: Membrane tension tends to decrease the radius of the protrusion, and thus pushes the filaments together into a tapered shape. We respectively denote by r_t , $r_t - \delta r_t$ and ℓ_t the largest radius, smallest radius and length of the tapered end. The membrane is represented in blue.

S2.1 Simplified master equation

In this section we establish Eqs. (8), (9) and (10) of the main text by writing a master equation for the case of a single filament bound to a wall in Sec. S2.1.1, and then showing in Sec. S2.1.2 that the espin variable can be eliminated out of it, so that the evolution of filament length probability distribution can be described by an independent set of equations.

S2.1.1 Full master equation

We denote by $\{e_i = 0 \text{ or } 1\}$ the variables representing the state of the potential espin-binding sites, with $e_i = 0$ ($e_i = 1$) denoting an empty (occupied) site at position i .

Let Z be an integer smaller than vt and $\{E_i\}$ a set of numbers equal to either 0 or 1. We recall that z is defined as the position of the filament's pointed end. The master equation describes the evolution of

$$\mathcal{P} \left[\{e_i = E_i\}_{i \in \mathcal{E}(Z,t)}, z = Z; t \right], \quad (\text{S1})$$

i.e. of the probability that the filament altitude z is equal to the integer Z and the espin variables e_i are equal to the E_i s at time t . Note that the probability of Eq. (S1) is a function of the E_i s with indices such that

$$i \in \mathcal{E}(Z, t), \quad (\text{S2})$$

where $\mathcal{E}(Z, t)$ is the set of active espin sites at time t for a filament with its pointed end in Z . The condition Eq. (S2) means that i is an integer satisfying the two following conditions:

- $i \geq Z + 1$. Indeed, all espins lower than the tip of the filament ($i < Z$) have to be off, as there is no actin filament for them to attach to. On the other hand, the espin in $i = Z$ must be on, otherwise the filament end cannot be in $z = Z$ (it would immediately depolymerize) and the

probability of Eq. (S1) vanishes. As a consequence of this, we consider that the detachment of the espin in z and the instantaneous depolymerization of the filament to the next occupied espin site are one and the same event.

- $i \leq vt$, as we do not consider what happens above the polymerization front. In the following, we consider a situation analogous to the case $P_0 = 1$ of the previous section, meaning that any espin at altitude $i = vt$ has a probability one of being on. Its subsequent evolution is described by the master equation.

Following this, the master equation for the probability of Eq. (S1) is concerned only with espin detachment/attachment events.

If $Z \leq vt - 1$, the master equation reads

$$\partial_t \mathcal{P} \left[\{e_i = E_i\}_{i \in \mathcal{E}(Z,t)}, z = Z; t \right] = -\mathcal{P} \left[\{e_i = E_i\}_{i \in \mathcal{E}(Z,t)}, z = Z; t \right] + \mathcal{K}^b + \mathcal{K}^u + \mathcal{D}. \quad (\text{S3})$$

The first term of the right-hand side of this equation is the probability current away from the $(\{E_i\}, Z)$ state due to the detachment of the espin holding the filament's pointed end at the altitude Z , which induces a depolymerization event. The term \mathcal{K}^b is the probability current due to espin binding events. It reads

$$\begin{aligned} \mathcal{K}^b = & k \sum_{j \in \mathcal{E}_1(\{E_i\}, Z, t)} \mathcal{P} \left[\{\dots, e_{j-1} = E_{j-1}, e_j = 0, e_{j+1} = E_{j+1}, \dots\}_{i \in \mathcal{E}(Z,t)}, z = Z; t \right] \\ & - k \sum_{j \in \mathcal{E}_0(\{E_i\}, Z, t)} \mathcal{P} \left[\{\dots, e_{j-1} = E_{j-1}, e_j = 0, e_{j+1} = E_{j+1}, \dots\}_{i \in \mathcal{E}(Z,t)}, z = Z; t \right], \end{aligned} \quad (\text{S4})$$

where $\mathcal{E}_0[\{E_i\}_{i \in \mathcal{E}(Z,t)}, Z, t]$ and $\mathcal{E}_1[\{E_i\}_{i \in \mathcal{E}(Z,t)}, Z, t]$ are the complementary subsets of $\mathcal{E}(Z, t)$ containing all indices j such that $E_j = 0$ and $E_j = 1$, respectively. Both terms of \mathcal{K}^b implicate the probabilities of states with the espin site j unoccupied, meaning that an espin is susceptible of binding in j . The first term represent binding events to sites such that $E_j = 1$ and therefore represents a probability influx to the $(\{E_i\}, Z)$ state. The second term, on the other hand, represents events where an espin binds to a site j such that $E_j = 0$ and thus represents a probability flux away from the $(\{E_i\}, Z)$ state. The term \mathcal{K}^u is the probability current due to espin unbinding events that do not induce any depolymerization (*i.e.* occurring at altitude $Z + 1$ or higher). It reads

$$\begin{aligned} \mathcal{K}^u = & \sum_{j \in \mathcal{E}_0(\{E_i\}, Z, t)} \mathcal{P} \left[\{\dots, e_{j-1} = E_{j-1}, e_j = 1, e_{j+1} = E_{j+1}, \dots\}_{i \in \mathcal{E}(Z,t)}, z = Z; t \right] \\ & - \sum_{j \in \mathcal{E}_1(\{E_i\}, Z, t)} \mathcal{P} \left[\{\dots, e_{j-1} = E_{j-1}, e_j = 1, e_{j+1} = E_{j+1}, \dots\}_{i \in \mathcal{E}(Z,t)}, z = Z; t \right], \end{aligned} \quad (\text{S5})$$

which has a similar interpretation to \mathcal{K}^b . The term \mathcal{D} stands for the probability current to the $(\{E_i\}, Z)$ state due to depolymerization events. It reads

$$\mathcal{D} = \sum_{Z'=-\infty}^{Z-1} \mathcal{P} \left[\{e_{Z'+1} = 0, \dots, e_{Z-1} = 0, e_Z = 1, e_{Z+1} = E_{Z+1}, \dots\}_{i \in \mathcal{E}(Z',t)}, z = Z'; t \right], \quad (\text{S6})$$

meaning that the depolymerization of a filament with its pointed end located at the altitude Z' results in an increase of the probability of the $(\{E_i\}, Z)$ state if and only if all espins between Z' and Z are off (*i.e.* the filament immediately depolymerizes to the position Z) and the espin is Z is on (*i.e.* depolymerization stops in Z).

We now turn to the boundary condition at the polymerization front, *i.e.* to the master equation for $vt - 1 < Z \leq vt$. At this location, none of the three first terms of the right-hand side of Eq. (S3) exist. Indeed, the filament is not allowed to depolymerize further than the polymerization front and there are no espin sites undergoing attachment/detachment events except for the one in Z . Denoting by $\lfloor x \rfloor$ the integral part (or floor) of any real number x , the master equation for the site closest to the polymerization front reads

$$\partial_t \mathcal{P} \left[\{e_i = E_i\}_{i \in \mathcal{E}(\lfloor vt \rfloor, t)}, z = \lfloor vt \rfloor; t \right] = \partial_t \mathcal{P} [z = \lfloor vt \rfloor; t] = \mathcal{D}'. \quad (\text{S7})$$

In this equation, the first equality reflects the fact that there are no active espin sites above $z = \lfloor vt \rfloor$ —otherwise said $\mathcal{E}(\lfloor vt \rfloor, t) = \emptyset$. The term \mathcal{D}' is a modified depolymerization current taking into account the fact that filaments cannot depolymerize beyond the polymerization front:

$$\begin{aligned} \mathcal{D}' &= \sum_{Z'=-\infty}^{\lfloor vt \rfloor - 1} \mathcal{P} \left[\{e_{Z'+1} = 0, \dots, e_{\lfloor vt \rfloor - 1} = 0\}_{i \in \mathcal{E}(Z', t)}, z = Z'; t \right] \\ &= \sum_{Z'=-\infty}^{\lfloor vt \rfloor - 1} \mathcal{P} \left[\{e_{Z'+1} = 0, \dots, e_{\lfloor vt \rfloor - 1} = 0, e_{\lfloor vt \rfloor} = 0\}_{i \in \mathcal{E}(Z', t)}, z = Z'; t \right] \\ &\quad + \mathcal{P} \left[\{e_{Z'+1} = 0, \dots, e_{\lfloor vt \rfloor - 1} = 0, e_{\lfloor vt \rfloor} = 1\}_{i \in \mathcal{E}(Z', t)}, z = Z'; t \right]. \end{aligned} \quad (\text{S8})$$

This probability has exactly the same interpretation as \mathcal{D} , except that depolymerization cannot continue beyond $Z = \lfloor vt \rfloor$ and stops there whatever the state of the espin site *i.e.* whatever the value of $e_{\lfloor vt \rfloor}$.

The master equation is now completely specified, but the initial state of the system is not. In the following, we consider a slight generalization of the case discussed in Eqs. (8), (9) and (10). We look at situations where the system is prepared at $t = 0$ in a superposition of states where the position $Z_0 \leq 0$ of the filament tip is well-defined, and the probabilities for the espin sites between $Z_0 + 1$ and 0 to be occupied are arbitrary, although independent from one another [Eqs. (8), (9) and (10) correspond to the special case $Z_0 = 0$]. Here we denote the initial probability for the espin site in i to be on by $\frac{k + \delta_0(i)}{1 + k}$, where the $\{\delta_0(i)\}_{i \in \{Z_0 + 1 \dots -1\}}$ are arbitrary numbers to be specified depending on the particular problem at hand and $\delta_0(0) = 1$, meaning that the espin site located at the polymerization front is occupied. Here the notation $\{i \dots j\}$ with $(i, j) \in \mathbb{N}^2$ stands for the integer interval comprising i, j and all integers in between. Leaving the filament dynamics aside, it is fairly obvious that the probability for an espin site to be occupied when at equilibrium with the espin reservoir is $\frac{k}{1 + k}$. Therefore $\delta_0(i)$ represents the deviation of the state of site i away from equilibrium. Following this discussion, the initial state is given by

$$\mathcal{P} \left[\{e_i = E_i\}_{i \in \mathcal{E}(Z, t)}, z = Z; t = 0 \right] = \left[\prod_{j \in \mathcal{E}_0(\{E_i\}, Z, 0)} \frac{1 - \delta_0(j)}{1 + k} \right] \left[\prod_{j \in \mathcal{E}_1(\{E_i\}, Z, 0)} \frac{k + \delta_0(j)}{1 + k} \right] \delta_{Z, Z_0}, \quad (\text{S9})$$

where the symbol δ_{Z, Z_0} denotes the Kronecker delta.

S2.1.2 Integrating espin out of the master equation

The problem specified in the previous section is at first sight a very complicated one, since it deals with a system whose state is specified by a large number of variables: the filament end position z , and $\lfloor vt - z \rfloor$ additional espin variables. In this section, we show that if an initial condition of

the form of Eq. (S9) is used, this dynamics simplifies considerably and it is possible to write an effective master equation in a closed form for the filament height probability

$$P(Z, t) = \sum_{\{E_i=0,1\}_{i \in \mathcal{E}(Z,t)}} \mathcal{P} \left[\{e_j = E_j\}_{j \in \mathcal{E}(Z,t)}, z = Z; t \right], \quad (\text{S10})$$

where the sum is over all possible values of the espin variables.

In order to prove this, we introduce the quantity

$$\mathcal{Q} \left[\{E_i\}_{i \in \mathcal{E}(Z,t)}, Z; t \right] = \left[\prod_{j \in \mathcal{E}_0(\{E_i\}, Z, t)} \frac{1 - \delta(j, t)}{1 + k} \right] \left[\prod_{j \in \mathcal{E}_1(\{E_i\}, Z, t)} \frac{k + \delta(j, t)}{1 + k} \right] P(Z, t), \quad (\text{S11})$$

with $\delta(i, t) = \delta_0(i)e^{-(1+k)t}$. Here the $\{\delta_0(i)\}_{i \in \{Z_0+1..-1\}}$ are the same as the numbers defined in Eq. (S9). The $\{\delta_0(i)\}_{i \in \mathbb{N}}$, on the other hand, are new constants, the value of which we discuss in the following. The factor $e^{-(1+k)t}$ by which the $\delta_0(i)$ s are multiplied reflect the exponential relaxation of the espin sites towards a chemical equilibrium with the espin reservoir. Here we show that \mathcal{Q} is a solution of the master equation provided that the $\{\delta_0(i)\}_{i \in \mathbb{N}}$ are chosen properly and that $P(Z, t)$ obeys a system of equations to be specified.

There are two boundary conditions to be considered on top of Eq. (S3). The first one concerns the espin variables and stipulates that if vt is an integer, the probability that the espin site located at the altitude $i = vt$ is equal to one ($P_0 = 1$). This condition reads

$$\mathcal{P}(e_i = 1; t = i/v) = \sum_{\{E_j=0,1\}_{j < i}} \sum_{Z=-\infty}^i \mathcal{P} \left[\{e_l = E_l\}_{l \in \mathcal{E}(Z,t)}, z = Z; t = i/v \right] = 1. \quad (\text{S12})$$

Using Eq. (S11) and the normalization condition

$$\sum_{Z \leq vt} P(Z, t) = 1, \quad (\text{S13})$$

we find that \mathcal{Q} satisfies Eq. (S12) if and only if

$$\forall i \in \mathbb{N} \quad \delta(i, i/v) = 1 \quad \Leftrightarrow \quad \forall i \in \mathbb{N} \quad \delta_0(i) = e^{(1+k)i/v}. \quad (\text{S14})$$

In the following, we use this condition as the definition of the $\{\delta_0(i)\}_{i \in \mathbb{N}}$. This implies

$$\forall i \in \mathbb{N} \quad \forall t \in \mathbb{R}^+ \quad \delta(i, t) = \exp \left[-(1+k) \left(t - \frac{i}{v} \right) \right]. \quad (\text{S15})$$

The second boundary condition is Eq. (S7), which \mathcal{Q} satisfies if and only if

$$\partial_t P(\lfloor vt \rfloor, t) = \sum_{Z'=-\infty}^{\lfloor vt \rfloor - 1} \left[\prod_{i=Z'+1}^{\lfloor vt \rfloor - 1} \frac{1 - \delta(i, t)}{1 + k} \right] P(Z', t). \quad (\text{S16})$$

We now consider the initial condition. It is obvious that \mathcal{Q} satisfies Eq. (S9) at $t = 0$ if and only if

$$P(Z, t = 0) = \delta_{Z, Z_0}. \quad (\text{S17})$$

Finally, we consider the master equation Eq. (S3) for a generic filament length $Z \leq vt - 1$. Inserting \mathcal{Q} into Eq. (S3), we find that the time derivatives of the two products in \mathcal{Q} simplify with \mathcal{K}^b and \mathcal{K}^u . We are thus left with the condition

$$\forall Z \in \{Z_0 \dots [vt-1]\} \quad \partial_t P(Z, t) = -P(Z, t) + \frac{k + \delta(Z, t)}{1 + k} \sum_{Z'=-\infty}^{Z-1} \left[\prod_{i=Z'+1}^{Z-1} \frac{1 - \delta(i, t)}{1 + k} \right] P(Z', t). \quad (\text{S18})$$

We discuss the interpretation of this equation in Sec. S2.1.4. Let us now prove more rigorously that $P(Z, t)$ is indeed the probability of finding the pointed end of the filament in Z at time t . The problem defined in Sec. S2.1.1 has a unique solution. On the other hand, the function \mathcal{Q} defined in Eqs. (S11) and (S15) is a solution of this problem if and only if $P(Z, t)$ satisfies the system constituted of Eqs. (S16), (S17) and (S18). Therefore, \mathcal{Q} is *the* unique solution of the problem defined in Sec. S2.1.1 if and only if the system Eqs. (S16), (S17) and (S18) has a solution that is normalized to one. This is true because of the following three reasons: this system is linear; $P(Z, t = 0)$ is normalized to one; and Eqs. (S16) and (S18) conserve probability. Thus we proved that \mathcal{Q} always exists, and is therefore the unique solution of the problem studied here.

In conclusion, solving the master equation of the one-filament problem is equivalent to solving the system of equations Eqs. (S16), (S17) and (S18), which are identical to Eqs. (8), (9) and (10) for $Z_0 = 0$.

S2.1.3 Qualitative meaning of the espin elimination

Here we reflect on the meaning of Eq. (S11). Using this equation, we find the conditional probability for the i th espin to be on assuming the filament tip is in Z ($i \in \{Z + 1 \dots [vt]\}$):

$$\mathcal{P}(e_i = 1 | z = Z; t) = \frac{\mathcal{P}(e_i = 1, z = Z; t)}{P(Z, t)} = \frac{k + \delta(i, t)}{1 + k}, \quad (\text{S19})$$

meaning that the state of the espin site in i is independent of the altitude z of the pointed end as long as $z < i$. This is the key to the simple form of \mathcal{Q} : in the process described here, all espins above the altitude of the filament's pointed end attach and detach independently from each other and from the filament dynamics. On the other hand, if the filament end is assumed to be at altitude Z , then the espin in Z is on with probability one, meaning that it is completely correlated with the filament, although uncorrelated with the other espins. Although this fact might seem obvious at first sight, one should note that this is only true in the special case considered here where the depolymerization rate of the filament is infinite. In the generic situation where depolymerization happens on a time scale comparable to that of the espin dynamics, the correlations between filaments and espin are not confined to the very last espin site anymore, but penetrate into the following sites. This situation is studied numerically in Ref. (6), and we propose that the case of large but finite depolymerization rates could be tackled by a perturbation scheme around the analytical results presented here.

S2.1.4 Interpretation of the simplified master equation

We now use the results of Sec. S2.1.3 to give a simple interpretation of the simplified master equation Eq. (S18). The first term of its right-hand side is the probability current away from the (Z) state (*i.e.* the state where the pointed end of the filament is in Z). The rate of escaping this state is 1, which is the detachment rate of the espin holding the filament in Z . The second term represents the probability influx to the (Z) state. This influx is due to filaments depolymerizing from any altitude $Z' < Z$ to the altitude Z , which is reflected by the sum over Z' . Just like a filament in Z ,

a filament in Z' has a rate 1 of depolymerizing, which is the off rate of the espin located at altitude Z' . Whether it is going to depolymerize all the way to the altitude Z depends on the state of the espins located between Z' and Z . Let us consider a filament with its pointed end in Z' that starts depolymerizing. It contributes to $\partial_t P(Z, t)$ under two conditions. First, all espins between Z' and Z have to be off, which happens with probability [see Eq. (S19)]

$$\frac{1 - \delta(Z' + 1, t)}{1 + k} \times \frac{1 - \delta(Z' + 2, t)}{1 + k} \times \dots \times \frac{1 - \delta(Z - 1, t)}{1 + k}. \quad (\text{S20})$$

Second, the espin in Z has to be on, which happens with probability $\frac{k + \delta(Z, t)}{1 + k}$. Since as shown in Sec. S2.1.3 the espins above the pointed end of the filament behave independently from each other, we just have to multiply these probabilities to account for the form of Eq. (S18).

S2.2 The no-reattachment probability distribution is a solution of the master equation

Here we show that the probability distribution of Eq. (3) is a stationary solution of the problem specified by Eqs. (S16) and (S18) [or equivalently Eqs. (8) and (9)] for $n = 1$ (single filament case), $k = 0$ (no espin reattachment) and $P_0 = 1$ (all espin sites are occupied at the polymerization front). Note that the initial condition Eq. (S17) [or equivalently Eq. (10)] need not be considered as it is irrelevant in the stationary state. In the coordinate system defined in Fig. 3, Eq. (3) yields the following probability for the altitude of the filament's pointed end to be at altitude Z or larger

$$P_f^{\geq}(Z, t) = \prod_{i=1}^{+\infty} \left[1 - e^{-\left(t - \frac{Z}{v} + \frac{i}{v}\right)} \right] = \sum_{Z'=Z}^{\lfloor vt \rfloor} P_f(Z', t), \quad (\text{S21})$$

where $P_f(Z)$ is the probability for the filament's pointed end to be exactly in $Z < \lfloor vt \rfloor$. In Sec. S2.2.1 we show that this probability distribution satisfies the bulk master equation Eq. (S18), then in Sec. S2.2.2 we show that it satisfies the boundary condition Eq. (S16).

S2.2.1 Bulk equation: satisfying Eq. (S18)

According to Eq. (S21), $P_f(Z)$ can be expressed as

$$P_f(Z, t) = P_f^{\geq}(Z, t) - P_f^{\geq}(Z + 1, t) = e^{-(t-Z/v)} P_f^{\geq}(Z, t). \quad (\text{S22})$$

We use Eqs. (S21) and (S22) to explicitly calculate the time derivative of $P_f(Z, t)$, which reads:

$$\partial_t P_f(Z, t) = P_f(Z, t) \left\{ -1 + \sum_{i=1}^{+\infty} \frac{\exp\left[-\left(t - \frac{Z}{v} + \frac{i}{v}\right)\right]}{1 - \exp\left[-\left(t - \frac{Z}{v} + \frac{i}{v}\right)\right]} \right\}. \quad (\text{S23})$$

The right-hand side of Eq. (S18) can be expressed as

$$\begin{aligned}
& -P_f(Z, t) + e^{-(t-Z/v)} \sum_{Z'=-\infty}^{Z-1} \left\{ \prod_{i=Z'+1}^{Z-1} [1 - e^{-(t-i/v)}] \right\} P_f(Z', t) \\
&= -P_f(Z, t) + e^{-(t-Z/v)} \sum_{Z'=-\infty}^{Z-1} \frac{\prod_{i=-\infty}^{Z-1} [1 - e^{-(t-i/v)}]}{\prod_{i=-\infty}^{Z'} [1 - e^{-(t-i/v)}]} P_f(Z', t) \\
&= -P_f(Z, t) + e^{-(t-Z/v)} \sum_{Z'=-\infty}^{Z-1} \frac{P_f^{\geq}(Z, t)}{P_f^{\geq}(Z'+1, t)} P_f(Z', t) \\
&= -P_f(Z, t) + P_f(Z, t) \sum_{Z'=-\infty}^{Z-1} \frac{\exp\left[-\left(t - \frac{Z'}{v}\right)\right]}{1 - \exp\left[-\left(t - \frac{Z'}{v}\right)\right]}. \tag{S24}
\end{aligned}$$

This is the same expression as in Eq. (S23) up to the change of dummy variable $Z' = Z - i$, thus proving that the probability distribution of Eq. (3) is a stationary solution of Eq. (S18) in the original reference frame.

S2.2.2 Boundary condition: satisfying Eq. (S16)

According to Eq. (S21), the probability for the filament's pointed end to be exactly in $z = \lfloor vt \rfloor$ is

$$P_f(\lfloor vt \rfloor, t) = P_f^{\geq}(\lfloor vt \rfloor, t) = \prod_{i=1}^{+\infty} \left[1 - e^{-\left(t - \frac{\lfloor vt \rfloor}{v} + \frac{i}{v}\right)} \right], \tag{S25}$$

where the first equality is due to the fact that the filament's pointed end cannot be any higher than $\lfloor vt \rfloor$.

The left-hand side of Eq. (S16) reads:

$$\partial_t P_f(\lfloor vt \rfloor, t) = P_f(\lfloor vt \rfloor, t) \sum_{i=1}^{+\infty} \frac{\exp\left[-\left(t - \frac{\lfloor vt \rfloor}{v} + \frac{i}{v}\right)\right]}{1 - \exp\left[-\left(t - \frac{\lfloor vt \rfloor}{v} + \frac{i}{v}\right)\right]}. \tag{S26}$$

Using Eqs. (S22) and (S25) we can express the right-hand side of Eq. (S16) in a similar way to what was done in Eq. (S24):

$$\begin{aligned}
& \sum_{Z'=-\infty}^{\lfloor vt \rfloor - 1} \left\{ \prod_{i=Z'+1}^{\lfloor vt \rfloor - 1} [1 - e^{-(t-i/v)}] \right\} P_f(Z', t) \\
&= \sum_{Z'=-\infty}^{\lfloor vt \rfloor - 1} \frac{P_f^{\geq}(\lfloor vt \rfloor, t)}{P_f^{\geq}(Z'+1, t)} P_f(Z', t) \\
&= P_f(\lfloor vt \rfloor, t) \sum_{Z'=-\infty}^{\lfloor vt \rfloor - 1} \frac{\exp\left[-\left(t - \frac{Z'}{v}\right)\right]}{1 - \exp\left[-\left(t - \frac{Z'}{v}\right)\right]}. \tag{S27}
\end{aligned}$$

This expression is equal to that of Eq. (S26), thus proving that for $n = 1$, $k = 0$ and $P_0 = 1$ the probability distribution of Eq. (3) is a stationary solution of the system of equations Eqs. (S16) and (S18), and therefore of the full problem formulated in the section Discrete Master Equation and Solution Far from the Polymerization Front of the main text.

S2.3 Exact solution at chemical equilibrium

According to Eq. (S19), the probability for the espin site located at altitude $i > z$ to be occupied is equal to $\frac{k+\delta(i,t)}{1+k}$. This allows us to extend our interpretation of $\delta_0(i)$ to $\delta(i,t)$, which we can now interpret as the deviation of the espin density at site i from the steady-state density $\frac{k}{1+k}$ corresponding to a situation where site i is in equilibrium with the espin reservoir. Depending on the value of i , this imbalance can have two distinct origins. For $i \in \{Z_0 + 1 \dots -1\}$, it originates in the arbitrarily chosen initial state of the espin site, which is reflected by our choice of the $\{\delta_0(i)\}_{i \in \{Z_0+1 \dots -1\}}$. For $i \geq 0$, it comes from the fact that espin sites are always occupied at the polymerization front (they are incorporated into the actin bundle with probability one). With time, however, espin sites lose the memory of their initial conditions, and relax back to an equilibrium with the espin reservoir. This is reflected by the fact that for $i < 0$, $\delta(i,t) = \delta_0(i)e^{-(1+k)t}$ relaxes to zero at large times and that for $i \geq 0$, $\delta(i,t)$ vanishes far away from the polymerization front [*i.e.* for $vt - i \gg v/(1+k)$ —see Eq. (S15)].

In this section, we tackle the effective dynamics of the pointed end in a situation where all espins are in chemical equilibrium with the bulk, which is valid for long times and far away from the polymerization front. Let us define Q by

$$P(Z, t) = \frac{Q(Z, t)e^{-t}}{(1+k)^{Z_0-Z}}. \quad (\text{S28})$$

Here the boundary condition Eq. (S16) need not be considered as the polymerization front is assumed to be far away. Thus we only need to solve the system constituted by Eqs. (S17) and (S18), which now read

$$Q_e(Z, t = 0) = \delta_{Z, Z_0} \quad (\text{S29a})$$

$$\partial_t Q_e(Z, t) = k \sum_{Z'=-\infty}^{Z-1} Q_e(Z', t), \quad (\text{S29b})$$

where the index e denotes the fact that the espins are at equilibrium with the reservoir.

In Sec. S2.3.1 we establish a preliminary result, and use it in Sec. S2.3.2 to solve this system of equations. Finally, in Sec. S2.3.3 we write down the exact asymptotic (*i.e.* far away from the polymerization front) solution of the problem presented in the section Discrete Master Equation and Solution Far from the Polymerization Front of the main text, and derive its diffusive limit as presented in Eq. (11).

S2.3.1 Preliminary result

Let $(A, i) \in \mathbb{N}^{*2}$ with $i < A$. Here we prove the relationship

$$\sum_{j=1}^{A-i} \frac{i(A-j-1)!}{(A-j-i)!} = \frac{(A-1)!}{(A-i-1)!} \quad (\text{S30})$$

by recursion over A .

1. **Base case.** Let $A = i + 1$. In this case, Eq. (S30) reads

$$\sum_{j=1}^1 \frac{i(i+1-j-1)!}{(i+1-j-i)!} = \frac{(i+1-1)!}{(i+1-i-1)!}, \quad (\text{S31})$$

which is true as both sides of the equation are equal to $i!$.

2. **Recursion.** Assuming that the relationship Eq. (S30) is true for A , we establish it for $A + 1$. Incrementing A by one unit, the left-hand side of Eq. (S30) reads

$$\sum_{j=1}^{A+1-i} \frac{i(A-j)!}{(A+1-j-i)!} = \sum_{j'=0}^{A-i} \frac{i(A-j'-1)!}{(A-j'-i)!} = \frac{i(A-1)!}{(A-i)!} + \sum_{j'=1}^{A-i} \frac{i(A-j'-1)!}{(A-j'-i)!}, \quad (\text{S32})$$

where we made the change of dummy variable $j' = j - 1$. The right-hand side of Eq. (S30), on the other hand, reads

$$\frac{A!}{(A-i)!} = i \frac{(A-1)!}{(A-i)!} + (A-i) \frac{(A-1)!}{(A-i)!} = \frac{i(A-1)!}{(A-i)!} + \frac{(A-1)!}{(A-i-1)!}. \quad (\text{S33})$$

Using the recursion hypothesis shows that the last terms of Eqs. (S32) and (S33) are equal, thus establishing Eq. (S30) for all A s.

S2.3.2 Full solution

We now show that

$$Q_e(Z_0, t) = 1 \quad (\text{S34a})$$

$$Q_e(Z, t) = \sum_{i=1}^{Z-Z_0} \frac{(Z-Z_0-1)!}{(i-1)!(Z-Z_0-i)!} \frac{(kt)^i}{i!}, \quad (\text{S34b})$$

is a solution of Eqs. (S29). It obviously satisfies it in the special case $Z = Z_0$, as well as for $t = 0$. Injecting Eq. (S34b) in Eq. (S29b), redefining $i \rightarrow i + 1$ in the left-hand side and permuting sums in the right-hand side with $i = Z - Z'$, we find that the probability distribution of Eqs. (S36) is a solution of Eqs. (S29) if and only if

$$k + k \sum_{i=1}^{Z-Z_0-1} \frac{(kt)^i}{(i!)^2} \frac{(Z-Z_0-1)!}{(Z-Z_0-i-1)!} = k \sum_{i=1}^{Z-Z_0-1} \frac{(kt)^i}{(i!)^2} \sum_{j=1}^{Z-Z_0-i} \frac{i(Z-Z_0-j-1)!}{(Z-Z_0-j-i)!} + k. \quad (\text{S35})$$

This equality is proved by using Eq. (S30) with $A = Z - Z_0$.

S2.3.3 Chemical equilibrium probability distribution

Using Eq. (S28), Eq. (S34) yields

$$P_e(Z_0, t) = e^{-t} \quad (\text{S36a})$$

$$P_e(Z, t) = \frac{e^{-t}}{(1+k)^{Z_0-Z}} \sum_{i=1}^{Z-Z_0} \frac{(Z-Z_0-1)!}{(i-1)!(Z-Z_0-i)!} \frac{(kt)^i}{i!}, \quad (\text{S36b})$$

where it is understood in Eq. (S36b) that $Z > Z_0$ [note that $P(Z, t) = 0$ for $Z < Z_0$].

Eq. (S36) describes the depolymerization dynamics of the filament. Since Eq. (S29b) is invariant by both time and space translations, we expect that depolymerization takes place at a constant average velocity. Also, since depolymerization is a stochastic process, the initially peaked altitude distribution Eq. (S29a) broadens as time increases. These features are indeed observed of Fig. S2(a), where we plot the probability distribution P_e derived here. From an analytical point of view, the dynamics of the pointed end is expected to be diffusive on long length and time scales. We

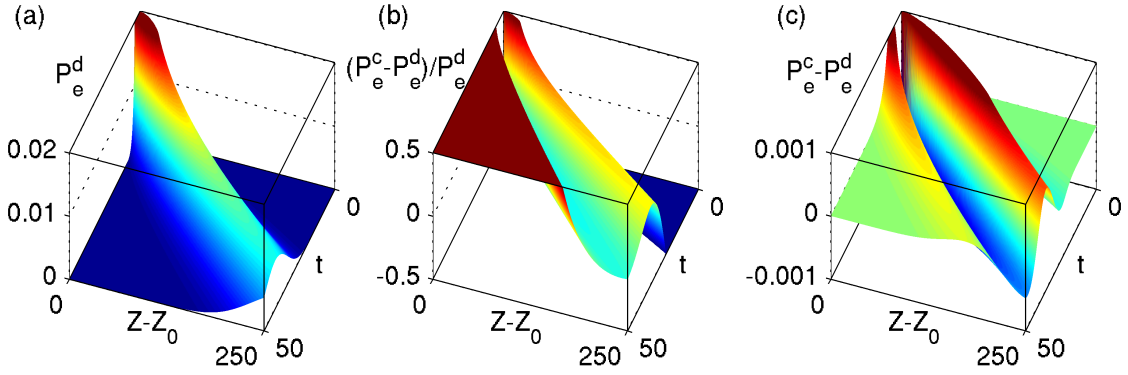


Figure S2: Probability distribution for the depolymerization of a filament cross-linked by espins at equilibrium with a reservoir characterized by $k = 0.2$. Here we denote by P_e^d the exact discrete solution given in Eqs. (S36) and by P_e^c the continuum approximation Eq. (S37). (a) Discrete solution plotted as a function of time and space. (b) Relative error $(P_e^c - P_e^d)/P_e^d$. Large values of the relative error are observed in regions where the probability is very small (*i.e.* in unimportant regions). (c) Absolute error $P_e^c - P_e^d$, where these seemingly large errors do not appear.

show this by considering the $t \rightarrow +\infty$ limit, where Stirling's approximation can be applied to the factorials of Eq. (S36) and the discrete sum can be replaced by an integral. Expanding the resulting expression to lowest order in $1/t$ in the scaling region defined by $\langle Z - Z_0 \rangle(t) = \mathcal{O}(t)$ and $\langle [(Z - Z_0) - \langle Z - Z_0 \rangle]^2 \rangle(t) = \mathcal{O}(t)$ yields a gaussian integral, which we compute to find

$$P_e(Z, t)_{t \rightarrow +\infty} \propto \exp \left\{ -\frac{k^2}{2(1+k)(2+k)t} \left[Z - Z_0 - \frac{(1+k)t}{k} \right]^2 \right\}, \quad (\text{S37})$$

which is equivalent to Eq. (11). It is in good agreement with the full, discrete solution for long times, as shown in Fig. S2(b-c).

S3 Long stationary filament with reattachment

Here we give the details of the calculations presented in the section Growth Transition and Stationary State of the main text.

In Sec. S3.1 we supplement the discussion of the section Growth Transition and Stationary State of the main text with a few more technical considerations and show that the master equation describing the single-filament depolymerization process cannot be mapped onto a Fokker-Planck equation in the continuum limit. We then extend the master equation to cases where a single filament is bound to several walls, in Sec. S3.2. In Sec. S3.3, we derive an appropriate continuum limit for this generalized master equation. The stationary solution of this problem is given in Sec. S3.4.

S3.1 Designing a continuum limit suitable for the study of the stationary state

Before taking on the derivation of a continuum limit for the master equation considered here, we need to discuss one more consequence of Eq. (14).

The section Stereocilium Shape Without Espin Reattachment of the main text mentions that the $v \rightarrow +\infty$ limit means that the stereocilium shape is smooth, and therefore that it can be

treated in some continuum limit. Sec. S2.3 demonstrates that on large length scales, the behavior of the pointed end can be assimilated to a particle diffusing in a locally homogeneous environment. It is tempting to extrapolate this result to the regions where espins are not in equilibrium with the reservoir. Doing so is actually a very common continuum approximation for one-dimensional stochastic processes, and is equivalent to approximating the master equation of Sec. S2.1.1 by a Fokker-Planck equation (*i.e.* a diffusion equation with position-dependent drift and diffusion coefficient) (7). From the considerations of the section Growth Transition and Stationary State, we however see that such an approximation is not valid. In order to understand this, we remind ourselves that there are *two* conditions of applicability of the Fokker-Planck approximation. The first one is that the scale over which the environment is inhomogeneous (in this case, the decay length $\frac{v}{1+k}$ of the espin density) must be much larger than the distance between two sites. This is the case as $\frac{v}{1+k} \gg 1$. But there is also a second one, which states that the size of the particle's jumps must be much smaller than the scale over which the environment is inhomogeneous. In our case, the jump size is the typical length d over which the filament depolymerizes in a single depolymerization event. According to the discussion of Growth Transition and Stationary State, $d = 1/\rho(\ell_s)$, where $\rho(\ell)$ is given by Eq. (12). Comparing d to $\frac{v}{1+k}$ and using Eqs. (13) and (14), we find

$$\frac{d(\ell_s)}{v/(1+k)} = \frac{1+k}{v\rho(\ell_s)} = 1+k \simeq 1. \quad (\text{S38})$$

Thus the jumps size is of the order of the length of the whole filament, and the Fokker-Planck approximation does not apply.

S3.2 Master equation with several walls for large v

Here we extend Eq. (S18) to the case where the filament is bound not to one, but to n walls, a situation pictured in Fig. 3(b). We do this in the limit $v \rightarrow +\infty$ with $\alpha = kv$ fixed, as discussed in the main text.

Building from our experience of stereocilia shapes acquired in the $k = 0$ case (section Stereocilium Shape Without Espin Reattachment) and noting that we are studying the case $P_0 = 1$, we are able to speculate that the upper section of the stereocilium is cylindrical over a length $v \ln v$, followed by a transition region (corresponding to the tapered region of the stereocilium) with a size of order v , which is the non-trivial part. In this region, $z \approx v \ln v \Rightarrow \delta(z, t) \approx e^{-(v \ln v)/v} \approx v^{-1}$. This implies that the probability for an espin site located in the transition region to be occupied is of order $\frac{k+e^{-\ln v}}{1+k} = \mathcal{O}(v^{-1})$. In other words, espins are scarce in the transition region.

Let us consider a filament with its pointed end at the altitude z belonging to the transition region and in contact with several walls, as illustrated in Fig. 3(b). The probability for at least one of the n espin sites located at altitude z to be occupied is equal to one, otherwise the filament would not be there. Because espins are scarce in the transition region, the probability to have two or more sites occupied in Z is smaller than that of having only one by a factor $\approx v^{-1}$. To lowest order in v^{-1} , we can therefore consider that the pointed end of the filament is held at the altitude z by exactly one espin.

Under this assumption, we can derive a master equation similar to Eq. (S18) using the same arguments as in Sec. S2.1.4. Here we present a qualitative justification for its form. Let $P(Z, t)$ be the probability that the pointed end of the filament is held in Z by any one of the espin sites located at this altitude. Like previously, the filament depolymerizes from this site with a rate 1. This means that the first term of Eq. (S18) is unchanged. If a filament is initially located in $Z' < Z$, it goes to Z upon detachment of the espin holding it in Z' on two conditions. First, all espin sites

between Z' and Z need to be empty, which happens with probability

$$\left[\frac{1 - \delta(Z' + 1, t)}{1 + k} \right]^n \times \left[\frac{1 - \delta(Z' + 2, t)}{1 + k} \right]^n \times \dots \times \left[\frac{1 - \delta(Z - 1, t)}{1 + k} \right]^n. \quad (\text{S39})$$

Second, at least one out of n espin sites in Z has to be occupied. This happens with probability

$$1 - \left[\frac{1 - \delta(Z, t)}{1 + k} \right]^n. \quad (\text{S40})$$

Following these arguments, the master equation for a filament bound to n walls for $v \gg 1$ and in the transition region reads:

$$\partial_t P(Z, t) = -P(Z, t) + \left\{ 1 - \left[\frac{1 - \delta(Z, t)}{1 + k} \right]^n \right\} \sum_{Z'=-\infty}^{Z-1} \left\{ \prod_{i=Z'+1}^{Z-1} \left[\frac{1 - \delta(i, t)}{1 + k} \right]^n \right\} P(Z', t), \quad (\text{S41})$$

where $Z_0 \leq Z < vt$. Note that the approach of this section is valid only in the transition region, which is very far away ($\approx v \ln v$) from the polymerization front in the $v \rightarrow +\infty$ limit. Therefore the boundary condition Eq. (S16) is irrelevant here. In the $v \rightarrow +\infty$ limit, $\delta(Z, t) \approx \delta(i, t) \approx k \approx v^{-1}$. Using the same level of approximation that we used when reasoning on the scarcity of espins, we expand the master equation to lowest order in v^{-1} :

$$\partial_t P(Z, t) = -P(Z, t) + n [k + \delta(Z, t)] \sum_{Z'=-\infty}^{Z-1} \left\{ \prod_{i=Z'+1}^{Z-1} [1 - n\delta(i, t) - nk] \right\} P(Z', t). \quad (\text{S42})$$

S3.3 Continuum limit for the master equation

According to the arguments of Sec. S3.1, the limit $v \rightarrow +\infty$ with $\alpha = kv$ fixed can also be understood as a continuum limit for the master equation Eq. (S42). This means that we are studying a situation where the typical decay length of the espin probability of presence is much larger than the distance between two cross-linkers, *i.e.* $v \gg 1$. In the stationary regime, the filament tip probability distribution depends only on the coordinate $\ell = vt - Z$. We define the coordinate ξ by

$$\ell = vt - Z = v \ln v + v\xi. \quad (\text{S43})$$

Since we are considering the transition region of the filament, *i.e.* a region of size $\approx v$ located at $\ell \approx v \ln v$, we consider only the region where ξ is of order 1. In the $v \rightarrow +\infty$ limit, we should thus be able to derive a v -independent shape equation for the transition region as a function of ξ . We therefore write the stationary filament length probability distribution as $P(\xi) = P(Z, t)$. According to Eq. (S43), $\partial_t P(Z, t) = dP(\xi)/d\xi$, and the prefactor of the last term of Eq. (S42) has the following asymptotic behavior

$$n [k + \delta(Z, t)] \underset{v \rightarrow +\infty}{\sim} nv \left(\alpha + e^{-\xi} \right). \quad (\text{S44})$$

Meanwhile, the sum behaves as

$$\sum_{Z'=-\infty}^{Z-1} \underset{v \rightarrow +\infty}{\sim} \int_{\xi}^{+\infty} \frac{d\xi'}{v}. \quad (\text{S45})$$

We also note that the product of Eq. (S42) has a finite limit:

$$\begin{aligned}
\prod_{i=Z'+1}^{Z-1} [1 - n\delta(i, t) - nk] &= \exp \left\{ \sum_{i=Z'+1}^{Z-1} \ln \left[1 - ne^{-(1+\alpha/v)(t-i/v)} - \frac{n\alpha}{v} \right] \right\} \\
&= \exp \left\{ \int_{v\xi}^{v\xi'} \left[\ln \left(1 - \frac{ne^{-y/v}}{v} - \frac{n\alpha}{v} \right) + \mathcal{O}(v^{-2}) \right] dy + \mathcal{O}(v^{-1}) \right\} \\
&= \frac{\exp(n\alpha\xi - ne^{-\xi})}{\exp(n\alpha\xi' - ne^{-\xi'})} [1 + \mathcal{O}(v^{-1})], \tag{S46}
\end{aligned}$$

where $vt - Z' = v \ln v + v\xi'$. Finally, we are able to write the $v \rightarrow +\infty$ continuum limit of the master equation Eq. (S42):

$$\frac{dP}{d\xi}(\xi) = -P(\xi) + n \left(\alpha + e^{-\xi} \right) \exp(n\alpha\xi - ne^{-\xi}) \int_{\xi}^{+\infty} \frac{P(\xi')}{\exp(n\alpha\xi' - ne^{-\xi'})} d\xi'. \tag{S47}$$

S3.4 Continuum solution for the stationary state

In this section we fully solve Eq. (S47), and show that it has a unique normalized solution. We define the function $f(\xi)$ by

$$P(\xi) = f(\xi) \times \exp \left[-(1 - n\alpha)\xi - ne^{-\xi} \right]. \tag{S48}$$

We divide Eq. (S47) by $n(\alpha + e^{-\xi}) \exp(n\alpha\xi - ne^{-\xi})$, differentiate with respect to ξ and make the change of variable $x = e^{-\xi}$. This yields

$$x(x + \alpha)f''(x) - [x - 2(x + \alpha) + n(x + \alpha)^2] f'(x) = 0. \tag{S49}$$

This second order linear differential equation has two linearly independent solutions, one of which is obviously a constant. Integration of the fraction $f''(x)/f'(x)$ yields the second one. This finally yields

$$P(x) = c_1 x^{1-n\alpha} e^{-nx} + c_2 \left[-\alpha + x^{1-n\alpha} e^{-nx} \int^x (u^{n\alpha-1} e^{nu}) du \right], \tag{S50}$$

where c_1 and c_2 are arbitrary constants to be determined. Note that choosing the lower bound in the integral is equivalent to modifying the value of c_1 .

Since $\ell \geq 0$, the variable ξ is defined on the interval $\xi \in [-\ln v, +\infty[$. As $\ln v \rightarrow +\infty$ in the limit considered here, the normalization condition for the probability distribution reads:

$$\int_{-\infty}^{+\infty} P(\xi) d\xi = 1. \tag{S51}$$

Meanwhile, Eq. (S50) implies

$$P(\xi) \xrightarrow{\xi \rightarrow +\infty} -\alpha c_2, \tag{S52}$$

meaning that the normalization condition Eq. (S51) can only be fulfilled if $\alpha = 0$ or $c_2 = 0$. If $\alpha = 0$ then

$$P(\xi) = \exp \left(-\xi - ne^{-\xi} \right) \left[c_1 + c_2 \int^{e^{-\xi}} \frac{e^{-nu}}{u} du \right]. \tag{S53}$$

The asymptotic behavior of the integral in this expression is given by

$$\int^x \frac{e^{-nu}}{u} du \underset{x \rightarrow +\infty}{\sim} \frac{e^{-nx}}{nx}. \quad (\text{S54})$$

Therefore if $\alpha = 0$ the probability density function has the following finite limit

$$P(\xi) \underset{\xi \rightarrow -\infty}{\rightarrow} \frac{c_2}{n}, \quad (\text{S55})$$

which prevents normalization unless $c_2 = 0$. Therefore c_2 always vanishes whatever the value of α .

Determining c_1 from the normalization condition Eq. (S51), the filament length distribution reads

$$P(\xi) = \frac{n^{1-n\alpha}}{\Gamma(1-n\alpha)} \exp\left[-(1-n\alpha)\xi - ne^{-\xi}\right], \quad (\text{S56})$$

where

$$\Gamma(b) = \int_0^{+\infty} \left(u^{b-1} e^{-u}\right) du \quad (\text{S57})$$

is the usual Gamma function (8). Qualitatively, the filament profiles described by Eq. (S56) are quite similar to those obtained in the absence of espin reattachment and described by Eq. (5). Indeed, $P(\xi)$ decays extremely quickly (faster than any exponential) for negative ξ s, while it decays as $e^{-(1-n\alpha)\xi}$ for $\xi \rightarrow +\infty$. By comparison, the distribution $P_f = -\frac{dP_{\leq}}{d\ell}$ [see Eq. (5)] decays as $e^{-\xi}$.

Eq. (4) relates the radius of the stereocilium to the probability that the filament is shorter than ξ . It is therefore interesting to write the cumulative probability distribution:

$$P_{\leq}(\xi) = \frac{\Gamma(1-n\alpha, ne^{-\xi})}{\Gamma(1-n\alpha)}, \quad (\text{S58})$$

where the incomplete Gamma function is defined as

$$\Gamma(b, x) = \int_x^{+\infty} \left(u^{b-1} e^{-u}\right) du. \quad (\text{S59})$$

The average filament length is given by

$$\langle \xi \rangle = \ln n - \psi(1-n\alpha) \quad \Leftrightarrow \quad \langle \ell \rangle = v \ln(nv) - v\psi(1-nkv), \quad (\text{S60})$$

where the digamma function and its behavior in 0 and 1 are given by (8)

$$\psi(z) = \frac{d[\ln \Gamma(z)]}{dz} \quad (\text{S61a})$$

$$\underset{z \rightarrow 0^+}{=} -\frac{1}{z} - \gamma + \mathcal{O}(z) \quad (\text{S61b})$$

$$\underset{z \rightarrow 1}{\rightarrow} -\gamma, \quad (\text{S61c})$$

where $\gamma \simeq 0.577216$ is the Euler constant. Similarly to Eq. (6), the transition region is at a distance $v \ln(nv)$ away from the polymerization front. Note that for $k = 0 \Leftrightarrow \alpha = 0$, Eq. (S58) goes to the distribution given in Eq. (5).

Differences with the $k = 0$ case (illustrated in Fig. 5) are observed when considering the width of the transition region, which is equal to $-v\psi(1-nkv)$. According to Eq. (S61b) this width diverges as

$$\langle \ell \rangle \underset{k \rightarrow k_c^-}{\sim} \frac{v}{1-nkv} \propto \frac{1}{|k - k_c|} \quad (\text{S62})$$

when k approaches the critical value

$$k_c = \frac{1}{nv}. \quad (\text{S63})$$

Therefore, for a large enough espin reattachment rate, a stationary filament profile ceases to exist. This is the n -walls generalization of the growth transition discussed in the beginning of the section Growth Transition and Stationary State. Indeed, for $k \geq k_c$, espin slows the depolymerization down so much that the pointed end can never catch up on the polymerization front.

S4 Coupling between filaments

S4.1 Numerical simulations

In order to implement the stereocilium dynamics as described in the section Model for the Actin and Cross-Linker Dynamics of the main text, we design a Monte-Carlo simulation based on the Gillespie algorithm (9). We simulate a square array of $L \times L$ filaments and denote the coordinates of a filament in the horizontal plane by (X, Y) . Each filament (X, Y) is connected to each of its four neighbors $(X \pm 1, Y)$, $(X, Y \pm 1)$ by an espin column [see Fig. 1(a)].

The altitude of the pointed end of filament (X, Y) is initially $Z_0(X, Y) = 0$, and is subsequently allowed to take any positive integer value smaller than vt , where t is the time elapsed since the beginning of the simulation. For each couple of neighboring filaments $\{(X, Y), (X + 1, Y)\}$ (or any other possible combination) and for each integer altitude i such that

$$\max[z(X, Y), z(X + 1, Y)] \leq i \leq vt, \quad (\text{S64})$$

there is an espin site $[(X, Y), (X + 1, Y), i]$, which can be either occupied or empty. Espins are incorporated with probability $P_0 = 1$ in $i = vt$. A filament with its pointed end in $z(X, Y)$ cannot depolymerize if there is an espin in at least one of the four following espin sites: $[(X, Y), (X \pm 1, Y), z(X, Y)]$, $[(X, Y), (X, Y \pm 1), z(X, Y)]$. Unlike in the model presented in the main text, if all those four sites are empty, the filament does not depolymerize instantaneously but does so with a finite rate k_d . In practice we set k_d to a very large value ($10^5 \times k_{\text{off}}$ or larger), therefore the simulation should yield the same results as the model presented in the section Model for the Actin and Cross-Linker Dynamics.

Two types of boundary conditions are used in our simulations. The first one is a periodic array of filaments, which is convenient when numerical simulations are used to investigate the $L \rightarrow +\infty$ limit. The second one is a circular array, where we impose that all filaments whose coordinates do not satisfy $(X - L/2)^2 + (Y - L/2)^2 < (L/2)^2$ are maximally depolymerized, and therefore that their pointed ends are always in $z = vt$. This allows us to simulate actual stereocilia more realistically. Example profiles from the simulations are shown in Fig. S3.

S4.2 Argument for the numerical value $n^{\text{eff}} = 2.5$

Here we give an argument for why the growth transition in a square ($n = 4$) array of filaments is well described by an effective number of neighboring walls $n^{\text{eff}} = 2.5$, as shown in Fig. 4. Let us consider a filament of length ℓ . As mentioned in the section Couplings Modify the Growth Transition of the main text, its pointed end's local environment is similar to that presented in Fig. 3(b), where neighboring filaments with a length larger or equal to ℓ play the role of walls. Denoting by $n^<$, $n^=$ and $n^>$ the typical numbers of neighbors with lengths smaller, equal to or larger than ℓ , this statement can be expressed as

$$n^{\text{eff}} = n^= + n^>. \quad (\text{S65})$$

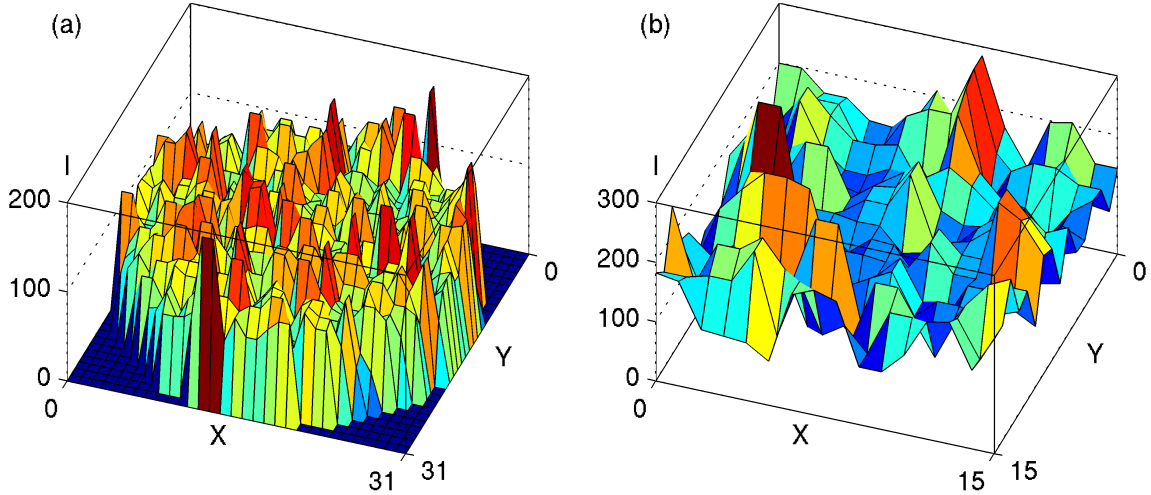


Figure S3: Profiles of two filament bundles obtained from the simulations described in the main text. The vertical axis represents the length $\ell = vt - z$ of the filaments, and was shrunk for easier visualization. In actual stereocilia, we expect the longest filaments to be brought together by the membrane as illustrated in Fig. S1. In this case, the stereocilium radius should be calculated as $r(\ell) \propto \sqrt{N^>(\ell)}$, where $N^>(\ell)$ is the number of filaments longer than ℓ —this is similar to Eq. (4). (a) 32×32 bundle with a circular support and $k = 0$. (b) 16×16 bundle with periodic boundary conditions and $k = 0.015$ —which we shown below to be a substantial reattachment rate, although below the growth transition. Both bundles are in their stationary state.

Let us now consider the appearance of the bundles pictured in Fig. S3. They have a markedly spiky appearance, which is further discussed in the next section. This implies that many filaments are sticking out of the bundle. Note however that a single filament cannot stick out on its own, as having no neighbor to cross-link its pointed end to causes immediate depolymerization. Indeed, the spikes observed in Fig. S3 are typically formed by two filaments of equal length cross-linked at their pointed end. From this typical situation we estimate

$$n^= = 1. \quad (\text{S66})$$

Now considering a pair (a, b) of neighboring filaments, it is obvious that if a is strictly longer than b , then b is strictly shorter than a . Summing over all pairs of neighboring filaments, this implies that the total number of longer neighboring filaments in the system is equal to the total number of shorter neighboring filaments, hence on average

$$n^< = n^>. \quad (\text{S67})$$

Finally, the total number of neighbors for any filament is equal to n , hence

$$n^< + n^= + n^> = n = 4. \quad (\text{S68})$$

Combining Eqs. (S65) to (S68) yields $n^{\text{eff}} = 2.5$, in agreement with the numerical results of Fig. 4.

S4.3 Correlations between filaments and interface width

The results of ‘Couplings modify the growth transition’ show that the behavior of coupled filaments below the growth transition is rather different from that of a single filament bound to several walls,

even if the number of walls is chosen to represent an effective number of longer neighbors. This anomalous behavior arises for the following reasons: in the $k = 0$, multi-filament case, the stochastic dynamics of each actin cross-linker is completely independent of the rest of the system. The actin filaments are slaved to the espins, and their dynamics is very simple. Therefore, correlations between the lengths of actin filaments are limited to nearest neighbors, since only filaments with a common actin cross-linker are coupled. In the case of a single filament with espin reattachment, on the other hand, the length of the filament influences the espin sites, as it determines whether a cross-linker can reattach or not. In multi-filament systems considered here, we expect filaments to be correlated over relatively long distances, as similar mutual correlations between filaments and espins mean that the state of a filament can now influence the neighboring espin column, which influences the next filament, and so on. In this section, we show that these correlations do indeed extend beyond the nearest neighbors, but present an argument suggesting that they are not sufficient to yield a self-affine interface.

Let us define the two-dimensional interface width function of the bundle as

$$w(X, Y) = \sqrt{\langle [\ell(X, Y) - \ell(0, 0)]^2 \rangle}. \quad (\text{S69})$$

This function reflects the amount of correlations between the heights of the filaments located in $(0, 0)$ and in (X, Y) . It is equal to 0 in the limit where the filaments are infinitely correlated, or if $X = Y = 0$. If the interface as a whole has a finite width $\sqrt{\langle \ell^2 \rangle - \langle \ell \rangle^2}$, then $w(X, Y)/\sqrt{2}$ goes to this value in the limit where the filaments are completely uncorrelated. Finally, $w(X, Y) > \sqrt{2}\sqrt{\langle \ell^2 \rangle - \langle \ell \rangle^2}$ represents a situation where the filaments are anticorrelated.

In Fig. S4(a), we present the normalized width function of a weakly cross-linked 32×32 filament bundle, which we define as

$$W(X, Y) = \frac{1}{\sqrt{2}} \frac{w(X, Y)}{\sqrt{\langle \ell^2 \rangle - \langle \ell \rangle^2}}. \quad (\text{S70})$$

The closer to one $W(X, Y)$ is, the less correlated the filaments are. Here the averages are over all filaments and over $\simeq 100$ time points of the bundle dynamics. The time between two time points is chosen to be larger than the time over which the length of the filaments are correlated. In other words, our time points can be considered as independent samples. We also make sure that all time points are taken after the bundle reaches its stationary state.

In Fig. S4(b), we collapse the data of this plot into a function of $R = \sqrt{X^2 + Y^2}$ and compare it with similar ones obtained for other values of k . We observe that the correlations between filaments decay as R increases. The precise functional form of this decay (*e.g.* whether it is exponential for large R) is difficult to assess from the data presented here, although a more thorough study could yield more information. Another related question is whether there is a well-defined correlation length associated with this decay, and how it behaves at the growth transition. For instance, one might venture that the correlation length could diverge as $k \rightarrow k_c^-$, similarly to what happens in second-order phase transitions. In the following we give a few scaling comments on the morphology of the interface, which allows us to return to these questions at the end of the present section.

It is well known that out-of-equilibrium surface growth problems similar to the one studied here can lead to rough interfaces. During the past two decades, extensive efforts have gone into characterizing this roughness in terms of the self-affine geometry of the interface (10, 11). In terms of the width function defined here, the self-affinity property means that when R is large, $w(R)$ grows as a well-defined power law

$$w(R) \underset{R \rightarrow +\infty}{\propto} R^\zeta, \quad (\text{S71})$$

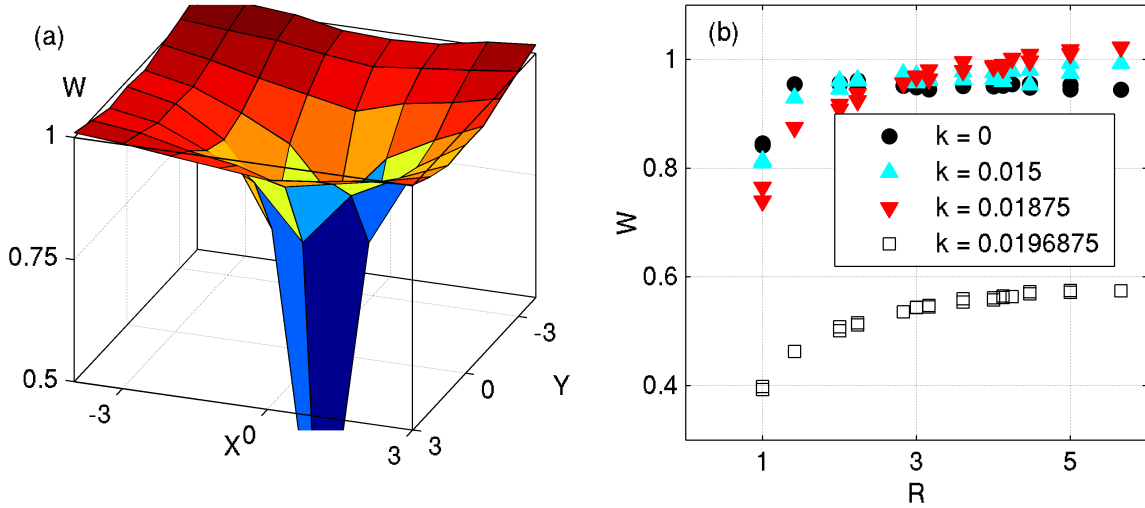


Figure S4: Normalized width functions $W(X, Y)$ for periodic filament bundles, as defined in Eq. (S70). (a) Two-dimensional normalized width function for a 8×8 periodic bundle with $k = 0.01875$. (b) Normalized width function plotted as a function of the distance R for 8×8 periodic bundles and for various values of k . The width function vanishes for $R = 0$ (not shown) by definition. For $k = 0$, the width is different from its asymptotic value only for $R = 1$, meaning that only nearest neighbors are correlated. For $k = 0.0196875$, the width of the interface never reaches 1 because correlations extend over the whole bundle, thus calling for simulations with a larger L .

which defines the roughness exponent $\zeta > 0$. Determining ζ —among other exponents—allows to define universality classes among out-of-equilibrium growth processes. Another type of behavior that can be characterized using the function $w(R)$ is the roughening transition of crystals (12). The width of a “rough” crystal interface diverges logarithmically, which corresponds to a roughness exponent $\zeta = 0$.

Here we discuss whether laws of the type of Eq. (S71) could apply to our stereocilium model for $k < k_c$. At first sight, the interface defined by the lengths of the filaments as a function of X and Y has similarities with both types of models, as it is both out-of-equilibrium and as its altitude can take only discrete values determined by the periodic arrangement of the cross-linkers in the vertical direction, which is similar to what happens in a crystal. We note however that two phenomena limit the divergence of the interface width expressed in Eq. (S71). First, the finite size of the bundle means that R cannot be larger than L . Second, even for $L \rightarrow +\infty$ the interfaces presented here have a finite width of order $\sqrt{\langle \ell^2 \rangle - \langle \ell \rangle^2}$. Indeed, the polymerization front traps them in the $\ell > 0$ half-space, and long filaments always tend to depolymerize if $k < k_c$, which keeps their lengths finite, although they might fluctuate to large values. The only way for us to apply the concepts presented in Eq. (S71) to stationary stereocilia is therefore to consider systems where L and $\sqrt{\langle \ell^2 \rangle - \langle \ell \rangle^2}$ are large (*i.e.* large bundles with k close to k_c) and study the shape of the interface in the domain where $1 \ll R \ll L$ and $1 \ll w(R) \ll \sqrt{\langle \ell^2 \rangle - \langle \ell \rangle^2}$. In other words, we are wondering whether we can make a statement about width functions of the type of those presented in Fig. S4(b) in the intermediate region where $(\langle \ell^2 \rangle - \langle \ell \rangle^2)^{-1/2} \ll W(R) \ll 1$. Here we prove by contradiction that no such region exists. Assume that there is a typical R scale, which we denote by R_0 , that has the properties

$$1 \ll R_0 \ll L \quad \text{and} \quad 1 \ll w(R_0) \ll \sqrt{\langle \ell^2 \rangle - \langle \ell \rangle^2}. \quad (\text{S72})$$

Moreover, we expect $w(R)$ to be an increasing function of R , as neighboring filaments should have more strongly correlated lengths than filaments far apart. Let (X, Y) and $(X + 1, Y)$ be two neighboring filaments with initially very similar heights $z(X, Y) \simeq z(X + 1, Y)$. Now consider that (X, Y) undergoes a depolymerization event. We saw in Eq. (S38) that the typical depolymerization length is $\langle \ell \rangle$, meaning that after the depolymerization event $z(X + 1, Y) - z(X, Y) \approx \langle \ell \rangle$. This kind of event is very common in our system, which implies that since $w(1) \approx z(X + 1, Y) - z(X, Y)$, we typically have $w(1) \approx \langle \ell \rangle$. As $w(R)$ is an increasing function of R , we have $w(R_0) \gtrsim \langle \ell \rangle$. From the previous sections we expect that $\langle \ell \rangle$ should be of order $v \ln v$ and $\sqrt{\langle \ell^2 \rangle - \langle \ell \rangle^2}$ of order v . Thus in the continuum limit $v \rightarrow +\infty$ considered here $\sqrt{\langle \ell^2 \rangle - \langle \ell \rangle^2} < \langle \ell \rangle$. Therefore, we finally find that $w(R_0) > \sqrt{\langle \ell^2 \rangle - \langle \ell \rangle^2}$, which is in contradiction with Eq. (S72).

In conclusion, in long stationary bundles of coupled filaments the interface reaches its maximum width $\sqrt{\langle \ell^2 \rangle - \langle \ell \rangle^2}$ over distances of order a few filaments, which means that it is impossible to define a mesoscopic scale where properties of the type described in Eq. (S71) could be observed. This accounts for the very spiky appearance of the profiles presented in Fig. S3. This also means that the width functions presented in Fig. S4(b) decay to a value very close to one on short length scales [$R = \mathcal{O}(1)$]. This argument seems to indicate that correlations between the filaments are smeared out by the large depolymerization jump sizes on length scales much smaller than the size of the system. It is therefore not obvious whether correlations could span the whole system, although Fig. S4(b) does seem to indicate that the typical correlation range grows as the growth transition is approached.

References

1. Fettiplace, R., and C. M. Hackney, 2006. The sensory and motor roles of auditory hair cells. *Nature Rev. Neurosci.* 7:19–29.
2. Derényi, I., F. Jülicher, and J. Prost, 2002. Formation and interaction of membrane tubes. *Phys. Rev. Lett.* 88:238101.
3. Itoh, M., 1982. Preservation and visualization of actin-containing filaments in the apical zone of cochlear sensory cells. *Hear. Res.* 6:277–289.
4. Sekerkova, G., L. Zheng, P. A. Loomis, E. Mugnaini, and J. R. Bartles, 2006. Espins and the actin cytoskeleton of hair cell stereocilia and sensory cell microvilli. *Cell. Mol. Life Sci.* 63:2329–2341.
5. Tilney, L. G., P. S. Connelly, L. Ruggiero, K. A. Vranich, and G. M. Guild, 2003. Actin filament turnover regulated by cross-linking accounts for the size, shape, location, and number of actin bundles in drosophila bristles. *Mol. Biol. Cell* 14:3953–3966.
6. Erlenkämper, C., 2008. Stochastische Beschreibungen dynamischer Biopolymere. Master’s thesis, Universität des Saarlandes.
7. Van Kampen, N. G., 1992. Stochastic Processes in Physics and Chemistry. North-Holland, Amsterdam.
8. Abramowitz, M., and I. A. Stegun, 1972. Handbook of Mathematical Functions. Number 55 in Applied Mathematics Series. National Bureau of Standards, Washington D. C.
9. Gillespie, D. T., 1976. A general method for numerically simulating the stochastic time evolution of coupled chemical reactions. *J. Comput. Phys.* 22:403.

10. Halpin-Healy, T., and Y.-C. Zhang, 1995. Kinetic roughening phenomena, stochastic growth, directed polymers and all that. Aspects of multidisciplinary statistical mechanics. *Phys. Rep.-Rev. Sec. Phys. Lett.* 254:215–414.
11. Barabási, A.-L., and H. E. Stanley, 1995. *Fractal Concepts in Surface Growth*. Cambridge University Press, Cambridge.
12. Nozières, P., 1992. *Solids Far from Equilibrium*. Cambridge University Press, Cambridge.